

# Shipborne observations reveal contrasting Arctic marine, Arctic terrestrial and Pacific marine aerosol properties

Jiyeon Park<sup>1</sup>, Manuel Dall'Osto<sup>2</sup>, Kihong Park<sup>3</sup>, Yeontae Gim<sup>1</sup>, Hyo Jin Kang<sup>1,4</sup>, Eunho Jang<sup>1,4</sup>, Ki-Tae Park<sup>1</sup>, Minsu Park<sup>5</sup>, Seong Soo Yum<sup>5</sup>, Jinyoung Jung<sup>1</sup>, Bang Yong Lee<sup>1</sup>, and Young Jun Yoon<sup>1,\*</sup>

<sup>1</sup>Korea Polar Research Institute, 26 Songdomirae-ro, Yeonsu-gu, Incheon 21990, South Korea

<sup>2</sup>Institut de Ciències del Mar, CSIC, Pg. Marítim de la Barceloneta 37-49, 08003, Barcelona, Catalonia, Spain

<sup>3</sup>Gwangju Institute of Science and Technology (GIST), 123 Cheomdangwagi-ro, Buk-gu, Gwangju 61005, Republic of Korea

<sup>4</sup>University of Science and Technology (UST), 217 Gajeong-ro, Yuseong-gu, Daejeon, Republic of Korea

<sup>5</sup>Department of Atmospheric Sciences, Yonsei University, 50 Yonsei-ro, Seodaemun-gu, Seoul 03722, Korea

\*Correspondence to: Y.J. Yoon (yjyoon@kopri.re.kr)

## Abstract

There are few shipborne observations addressing the factors influencing the relationships of the formation and growth of aerosol particles with cloud condensation nuclei (CCN) in remote marine environments. In this study, the physical properties of aerosol particles throughout the Arctic Ocean and Pacific Ocean were measured aboard the Korean ice breaker R/V Araon during the summer of 2017 for 25 days. A number of New Particle Formation (NPF) events and growth were frequently observed in both Arctic terrestrial and Arctic marine air masses. By striking contrast, NPF events were not detected in Pacific marine air masses. Three major aerosol categories are therefore discussed: (1) Arctic marine (aerosol number concentration  $CN_{2.5}$ :  $413 \pm 442 \text{ cm}^{-3}$ ), (2) Arctic terrestrial ( $CN_{2.5}$ :  $1622 \pm 1450 \text{ cm}^{-3}$ ) and (3) Pacific marine ( $CN_{2.5}$ :  $397 \pm 185 \text{ cm}^{-3}$ ), following air mass back trajectory analysis. A major conclusion of this study is that not only that the Arctic Ocean is a major source of secondary aerosol formation relative to the Pacific Ocean; but also that open ocean sympagic and terrestrial influenced coastal ecosystems both contribute to shape aerosol size distributions. We suggest that terrestrial ecosystems - including river outflows and tundra - strongly affects aerosol emissions in the Arctic coastal areas, possibly more than anthropogenic Arctic emissions. The increased river discharge, tundra emissions and melting sea ice should be considered in future Arctic atmospheric composition and climate simulations. The average CCN concentrations at a supersaturation ratios of 0.4% were  $35 \pm 40 \text{ cm}^{-3}$ ,  $71 \pm 47 \text{ cm}^{-3}$ , and  $204 \pm 87 \text{ cm}^{-3}$  for Arctic marine, Arctic terrestrial, and Pacific marine aerosol

30 categories, respectively. Our results aim to help to evaluate how anthropogenic and natural atmospheric  
31 sources and processes affect the aerosol composition and cloud properties.

32

### 33 **1. Introduction**

34 The climate change experienced in the Arctic is more rapid than that occurring at mid-latitudes in a  
35 phenomenon known as Arctic amplification (ACIA, 2005). In the warming Arctic, the extent and  
36 thickness of sea-ice have dramatically decreased over the past few decades (Stroeve et al., 2012). It has  
37 been estimated that the Arctic may seasonally become sea ice-free Arctic in the next 30 years (Wang  
38 and Overland, 2009). Aerosol particles in the atmosphere are a major driver of the Arctic climate (IPCC,  
39 2013), as they directly affect the climate through scattering and absorbing solar radiation (Stier et al.,  
40 2007), and indirectly by modifying the formation, properties, and lifetimes of clouds (Twomey, 1974).  
41 These direct and indirect effects are the leading uncertainty in current climate predictions. New particle  
42 formation (NPF), a predominant source of atmospheric particles, occurs through the formation of  
43 nanometer-sized molecular clusters ( $\sim 1$  nm) (i.e., nucleation) and their subsequent growth into aerosol  
44 particles of a few nanometers ( $\sim 1 - 10$  nm) and larger ( $\sim >10$  nm) (Kulmala et al., 2004; Zhang et al.,  
45 2012). NPF can significantly increase the number of aerosol particles in the atmosphere. During  
46 summer, the Arctic is more isolated from anthropogenic influences (Arctic Haze) and experiences  
47 comparatively pristine background aerosol conditions (Heintzenberg et al., 2015; Law and Stohl, 2007).  
48 As the number concentrations of particles in the Arctic during summer are very low (of an order of  $\sim 10^2$   
49  $\text{cm}^{-3}$ ) (Merikanto et al., 2009), the physicochemical properties of aerosol particles in the Arctic  
50 atmosphere is highly sensitive to NPF.

51 NPF events have been frequently observed within a wide range of environmental conditions at  
52 various Arctic locations, such as Zeppelin (Tunved et al., 2013; Croft et al., 2016; Heintzenberg et al.,  
53 2017), Tiksi (Asmi et al., 2016), Alert (Croft et al., 2016), Station Nord (Nguyen et al., 2016), and  
54 Barrow (Kolesar et al., 2017), and from limited ship-based observations (Chang et al., 2011; Kim et al.,  
55 2015; Heintzenberg et al., 2015). The formation and growth of particles in the Arctic atmosphere are

56 strongly influenced by marine, coastal, marginal ice, and/or anthropogenic sources. Oceanic dimethyl  
57 sulfide (DMS) and other volatile organic precursors (such as isoprene, monoterpenes, and amines) play  
58 important roles in the formation and growth of new particles in the Arctic (Leaitch et al., 2013; Willis et  
59 al., 2016; Park et al., 2017; Abbatt et al., 2019; Mungall et al., 2016). In addition, iodine oxides  
60 significantly contribute to NPF in marine and coastal Arctic environments owing to emissions from  
61 marine microalgae at low tide or snowpack photochemistry in [ice and snow-covered regions](#) (Allan et  
62 al., 2015; O'Dowd et al., 2002; Raso et al., 2017). Biogenic gaseous precursors released by the melting  
63 Arctic sea-ice margins have also been associated with NPF (Dall'Osto et al., 2017; Willis et al., 2018).  
64 Recent studies in Alaska have indicated that the formation and growth of particles are influenced by  
65 emissions from oil and gas extraction activities in Prudhoe Bay (Gunsch et al., 2017; Kolesar et al.,  
66 2017). Although several observations have been made in the Arctic under different environmental  
67 conditions ([Burkart et al., 2017b](#); [Collins et al., 2017](#)), there are few detailed size distribution analyses  
68 of particle formation and growth events within the Arctic marine environment.

69 Several studies have attempted to investigate the impacts of NPF on the concentrations of cloud  
70 condensation nuclei (CCN) (Willis et al., 2016; [Burkart et al., 2017b](#); [Collins et al., 2017](#)). Model-based  
71 studies have predicted that a large fraction of CCN (up to 78% of CCN at 0.2 % supersaturation) in the  
72 global atmosphere results from atmospheric NPF and growth (Merikanto et al., 2009; Westervelt et al.,  
73 2014; Spracklen et al., 2008). Field observations have also observed substantial increases in the  
74 concentrations of CCN due to atmospheric nucleation in various environments (Pierce et al., 2012;  
75 Kalivitis et al., 2015; [Burkart et al., 2017b](#); [Collins et al., 2017](#); Kim et al., 2019). [Several examples of  
76 increase in the CCN concentration after a few hours from the beginning of NPF events were presented  
77 by Burkart et al. \(2017b\) in the summer marine Arctic during the 2014 NETCARE Amundsen ice  
78 breaker campaign, by Kim et al \(2019\) at King Sejong Station in the Antarctic Peninsula, by Pierce et al.  
79 \(2012\) in a forested mountain valley in western Canada, and by Willis et al. \(2016\) in an Arctic aircraft  
80 campaign in Nunavut, Canada.](#) However, due to the infrequency of aerosol measurements collected  
81 onboard ice breakers, very few studies have measured the simultaneous aerosol size distribution and

82 CCN concentrations over the Arctic Ocean.

83 In this study, the physical characteristics of aerosol particles over the Arctic and Pacific Oceans were  
84 investigated between [August 31 and September 24, 2017](#), using aerosol particle monitoring instruments  
85 installed on the Korean ice breaker R/V Araon. Data of the aerosol size distribution, the concentrations  
86 of the total aerosol number (CN), black carbon (BC), and CCN were continuously collected using  
87 various aerosol instruments. The main aims of this study were to (1) investigate the frequency and  
88 characteristics of NPF and particle growth over the Arctic and Pacific Oceans, (2) determine the major  
89 sources that are associated with NPF based on backward air mass trajectory analysis, and (3) explore the  
90 potential contribution of NPF to the CCN concentrations in the remote marine environment.

91

## 92 **2. Experimental methods**

### 93 **2.1. Study area and ship tracks**

94 Ambient atmospheric aerosol measurements were collected over the Arctic and Pacific Oceans  
95 onboard the ice breaker R/V Araon, operated by the Korea Polar Research Institute (KOPRI), Korea.  
96 The ship's track is presented in Fig. 1. The cruises covered two main areas: the Arctic Ocean (including  
97 both Beaufort and Chukchi Seas) and the remote Northwest Pacific Ocean. The ship departed from  
98 Barrow, USA, on August 28, 2017, crossed the Beaufort (August 29-September 13, 2017) and Chukchi  
99 Seas (September 15, 2017), and reached Nome, USA, on September 16, 2017. The Beaufort Sea  
100 extends across the northern coasts of Alaska and the Northwest Territories of Canada. After completing  
101 the Arctic survey, the ship departed from Nome, USA, on September 18, 2017, crossed the Bering Sea,  
102 Sea of Okhotsk, and East Sea, and reached Busan, Korea, on September 28, 2017.

103

### 104 **2.2. Atmospheric aerosol measurements**

105 The aerosol sampling inlet was placed on the front deck of the ship (13 m above sea level), ahead of  
106 the ship's engines to avoid any influences from the emissions of the ship's exhaust. In addition, kitchen  
107 ventilation systems were connected by a plastic cylindrical pipe (~15 m length) and moved back on the

108 deck (far away from the sampling inlet) to minimize the potential effects of cooking emissions on the  
109 atmospheric measurements during the sampling periods. Aerosols were sampled through a stainless  
110 steel tube (inner diameter of 1/4 in, and length of ~1 m), which was connected to the various  
111 instruments by electrically conductive tubing to minimize particle losses in the sampling line.

112 The physical properties of the aerosols were measured with various aerosol instruments, including  
113 two condensation particle counters (TSI 3776 CPC and TSI 3772 CPC), two scanning mobility particle  
114 sizers (SMPS), an optical particle sizer (OPS), an aethalometer, and a cloud condensation nuclei counter  
115 (CCNC). The TSI 3776 CPC and TSI 3772 CPC measured the total number concentrations of particles  
116 larger than 2.5 and 10 nm every 1 sec, respectively. The aerosol sample flow rates of TSI 3776 CPC and  
117 TSI 3772 CPC were 1.5 and 1.0 lpm, respectively. The number size distributions of the particles were  
118 measured using the nano SMPS every 3 min (Differential mobility analyzer (DMA): TSI 3085, CPC:  
119 TSI 3776), covering a size range of 3 to 63.8 nm, and the standard SMPS (DMA: TSI 3081, CPC: TSI  
120 3772) every 3 min, covering a size range of 10 to 300 nm. The aerosol and sheath flow rates of the  
121 nano-SMPS were 1.5 and 15 lpm, respectively; and those of the standard SMPS were 1.0 and 10 lpm,  
122 respectively. An OPS (TSI 3330) was used to determine the size distribution of particles in the range of  
123 100 nm to 10  $\mu\text{m}$  diameter with a sample flow rate of 1.0 lpm every 3 minutes. The BC concentration  
124 was measured using an aethalometer (AE22, Magee Scientific Co., USA) with a 5-min time resolution  
125 to assess the influence of anthropogenic sources (such as local pollution and ship emissions). The  
126 instrument uses the absorption of light at a wavelength of 880 nm by the ambient aerosols collected on a  
127 quartz filter tape to determine the BC concentration. The flow rate through a sharp-cut 2.5  $\mu\text{m}$  cyclone  
128 (BGI, Inc., USA) was set to 5 lpm and the integration time was 5 min. The Droplet Measurement  
129 Technologies CCN counter (DMT CCN-100) was operated to measure the CCN number concentrations.  
130 The total flow rate in the CCN counter was 0.5 lpm, and the counter was operated at five different  
131 supersaturation ratios (SS) (0.2, 0.4, 0.6, 0.8, and 1.0 %) every 30 min. The sample and sheath flow  
132 rates of the CCN counter were 0.05 and 0.45 lpm, respectively.

### 2.3. Identification of ship exhaust

To obtain a data set that reflects background aerosol loading, measurement data affected by the exhaust emissions of the ship's engine should be excluded prior to further data analysis. For this, aerosol data were filtered based on the BC concentration, wind direction, wind speed, and total particle number concentration. The data with the following properties were discarded: (1) BC concentrations exceeding  $100 \text{ ng m}^{-3}$ , (2) relative wind direction against the ship's heading between  $110^\circ$  and  $260^\circ$ , as this originates directly from the ship's exhaust, (3) relative wind speed lower than  $2 \text{ m sec}^{-1}$  as air masses under a calm environment could become contaminated due to local turbulence, and (4) the total particle number concentrations were particularly high (spike) and varied dramatically in a short time. Ship plumes were clearly observed in the data collected during the campaign. The data collected when total aerosol number concentrations were higher than  $8000 \text{ cm}^{-3}$  were removed. In addition, the CPC and SMPS data were removed for the time periods when total aerosol number concentrations suddenly increased more than two times higher than the background values. Typically, the ship exhaust differs from the NPF events as the enhanced number concentration during the NPF events lasted for at least an hour with a low BC concentration (Ehn et al., 2010).

### 2.4. Backward air mass trajectory and satellite observations

The backward air mass trajectories were analyzed using version 4 of the Hybrid Single-Particle Lagrangian Integrated Trajectory (HYSPLIT) model (<http://ready.arl.noaa.gov/>) to examine their relationships with the physical characteristics of aerosol particles. The 2-day air mass back trajectories (48 h) were determined at hourly intervals from the ship's position at an arrival height of 50 m to estimate the transport history of the air masses arriving at the observation site (Park et al., 2018). The potential origins of the aerosols were divided into three categories based on the retention time of the 2-day back trajectories over the three major domains: Arctic Ocean (including the Beaufort and Chukchi Seas, and sea-ice region), Pacific Ocean (including the Bering Sea and Sea of Okhotsk) and land (including Alaska and the eastern part of Siberia) (Fig. 1). The phytoplankton biomass was obtained by

160 calculating the chlorophyll-*a* concentration from the level-3 product of Aqua Moderate Resolution  
161 Imaging Spectroradiometer at a 4 km resolution (Fig. S1). Geographical information over the ocean,  
162 land and sea-ice was obtained from the sea-ice index, which was provided by the National snow and Ice  
163 Data Center (NSIDC) (Fig. S2). Note that the sea-ice extent was defined as the area having an ice  
164 concentration of  $\geq 15\%$  (Pang et al., 2018). Air masses that intensively passed over the Beaufort and  
165 Chukchi Seas and sea-ice region were categorized as Arctic Ocean originated air masses (i.e.,  $> 50\%$   
166 retention over the ocean  $> 65^\circ\text{N}$  and sea-ice region). Air masses that intensively passed over Northern  
167 Alaska and the eastern Siberia were potentially affected by the Arctic tundra and categorized as land  
168 originated air masses (i.e.,  $> 50\%$  retention over the land domain). Finally, air masses that traveled  
169 through the Bering Sea and Sea of Okhotsk were categorized as air masses originated from Pacific  
170 Ocean domain (i.e.,  $> 50\%$  retention over the ocean domain  $< 65^\circ\text{N}$ ).

## 171 172 **2.5. Oceanic measurements**

173 To examine the influence of oceanic conditions on NPF and growth, seawater samples were collected  
174 from sea surface at a depth of  $\sim 1$  m by Niskin bottles. The sampling locations and methods have been  
175 described previously in more detailed (Park et al., 2019). In brief, concentrations of dissolved organic  
176 carbon (DOC) were measured with a Shimadzu TOC-V high-temperature combustion total organic  
177 carbon analyzer. To identify the source and composition of DOC in surface seawater, three-dimensional  
178 excitation-emission matrixes (EEMs) were scanned using a fluorescence spectrometer (Varian, USA).  
179 The excitation wavelength range was between 250 and 500 nm, and emission between 280 and 600 nm.  
180 In this study, the four major fluorescent components were classified into 4 groups; terrestrial humic  
181 substances peak (A) (EX: 260 nm, EM: 380–460 nm), the terrestrial fulvic substances peak (C) (EX:  
182 350 nm, EM: 420–480 nm), the marine fulvic substances peak (M) (EX: 312 nm, EM: 380–420 nm),  
183 and the proteinaceous peak (T) (EX: 275 nm, EM: 340 nm) (Coble, 2007).

## 184 185 **3. Results and discussion**

### 186 3.1. Overall particle number concentrations

187 Fig. 2a presents a time series of the 1 hour average total particle number concentration (CN)  
188 measured using TSI 3776 CPC and TSI 3772 CPC throughout the sampling periods. The number  
189 concentration of particles larger than 2.5 nm (CN<sub>2.5</sub>) or 10 nm (CN<sub>10</sub>) in the Arctic and Pacific marine  
190 environments had a range of approximately three orders of magnitude ( $\sim 10^1 - 10^3 \text{ cm}^{-3}$ ). In most cases,  
191 the CN<sub>2.5</sub> and CN<sub>10</sub> concentrations were less than  $\sim 2000 \text{ cm}^{-3}$ , with averages of  $505 \pm 280$  and  $492 \pm$   
192  $264 \text{ cm}^{-3}$ , respectively, which were in agreement with those reported in previous studies conducted at  
193 other Arctic stations (Asmi et al., 2016; Burkart et al., 2017a; Freud et al., 2017) and remote marine  
194 regions (O'Dowd et al., 2014; Sellegri et al., 2006; Kim et al., 2019; Jang et al., 2019; Yum et al., 1998;  
195 Hudson and Yum, 2002). For example, four years of observational data from the Arctic Climate  
196 Observatory in Tiksi, Russia, showed that the monthly median CN concentration ranged from  $\sim 184 \text{ cm}^{-3}$   
197 in November to  $\sim 724 \text{ cm}^{-3}$  in July (Asmi et al., 2016). Furthermore, Sellegri et al. (2006) reported CN  
198 concentrations under clean marine sector conditions at Mace Head of a few hundreds of  $\text{cm}^{-3}$  (e.g.,  $\sim 200$   
199  $\text{cm}^{-3}$  in January and  $\sim 450 \text{ cm}^{-3}$  in June). Elevated CN<sub>2.5</sub> and CN<sub>10</sub> concentrations were concentrated over  
200 the period from September 13 to 20, when the ship sailed over Chukchi and Bering Seas. During this  
201 period, CN<sub>2.5</sub> and CN<sub>10</sub> concentrations exceeding  $\sim 2000 \text{ cm}^{-3}$  were frequently observed. The peak  
202 concentrations of aerosol particles were notable, as the CN<sub>2.5</sub> and CN<sub>10</sub> concentrations exceeded  $\sim 6016$   
203 and  $\sim 5750 \text{ cm}^{-3}$ , respectively.

204 To elucidate further details of the variations in CN<sub>2.5</sub> and CN<sub>10</sub>, the particle size distributions  
205 measured with the nano SMPS, standard SMPS, and OPS were divided into four size groups: nucleation  
206 (3 – 20 nm), Aitken (20 – 100 nm), accumulation (100 – 300 nm), and coarse ( $> 300 \text{ nm}$  from OPS), as  
207 shown in Fig. 2b–e. The average number concentrations of the nucleation-mode (N<sub>NUC</sub>), Aitken-mode  
208 (N<sub>AIT</sub>), accumulation-mode (N<sub>ACC</sub>), and coarse-mode (N<sub>OPS</sub>) particles were  $169 \pm 142$ ,  $201 \pm 131$ ,  $40 \pm$   
209  $17$ , and  $4 \pm 2 \text{ cm}^{-3}$ , respectively. The temporal variations in N<sub>NUC</sub> and N<sub>AIT</sub> exhibited a distinct pattern,  
210 compared to that of N<sub>ACC</sub> and N<sub>OPS</sub>. Overall, N<sub>NUC</sub> and N<sub>AIT</sub> concentrations larger than  $\sim 1000 \text{ cm}^{-3}$  were  
211 observed from September 13 to 20 (e.g. the ship sailed over Chukchi and Bering Seas), whereas

212 relatively high concentrations of  $N_{ACC}$  and  $N_{OPS}$  were observed from September 21 to 23 (e.g., the ship  
213 sailed over Sea of Okhotsk). As shown in Fig. 2b, sudden bursts of nucleation-mode particles occurred  
214 frequently, as indicated by a sudden increase in the  $N_{NUC}$  concentration rising from tens to several  
215 thousands of  $cm^{-3}$ . Whenever the  $CN_{2.5}$  concentration exceeded  $\sim 2000\ cm^{-3}$ , the  $N_{NUC}$  concentration  
216 exceeded  $\sim 600\ cm^{-3}$  (except for the results observed in the evening of September 18). In addition, the  
217  $CN_{2.5}$  concentration was strongly correlated with the  $N_{NUC}$  concentration ( $r^2 = 0.69$ ) (Fig. S3),  
218 suggesting that the high CN concentration was mainly derived from nucleation-mode particles.  
219 Instances of elevated  $N_{NUC}$  occurred along the northern coast of Alaska (September 13 – 14, 2017),  
220 throughout the Chukchi Sea (September 15, 2017), near the Nome and Eastern Siberia (September 16 –  
221 18, 2017), and throughout the Bering Sea (September 19 – 20, 2017). During the cruises, the satellite-  
222 derived chlorophyll-*a* concentration data indicated strong biological activity over the Chukchi and  
223 Bering Seas, as shown in Fig. S1. Thus, the high occurrence of nucleation-mode particles may be  
224 related to multiple processes that influence the formation of secondary aerosols (e.g., oceanic biological  
225 activities, regional anthropogenic emissions on land (Alaska or eastern Siberia), and terrestrial sources  
226 in the tundra ecosystems of Alaska).

227

### 228 **3.2. Case studies**

229 As mentioned in Section 3.1, significant increases in  $N_{NUC}$  were frequently observed during the  
230 cruise (Fig. 2 b). Typically,  $N_{NUC}$  is used to indicate the presence of newly formed particles produced by  
231 gas-to-particle conversion (i.e., secondary aerosol formation) (Asmi et al., 2016; Burkart et al., 2017a).  
232 Here, an NPF event was defined as a sharp increase in the  $N_{NUC}$  with elevated  $CN_{2.5}$  that lasted for at  
233 least one hour. Fig. 3 presents contour plots of the size distributions measured using nano SMPS and  
234 standard SMPS. This strong NPF and growth event occurred over the Chukchi and Bering Seas, which  
235 border the western and northern sides of Alaska, suggesting that there may be a substantial source of  
236 precursors in this region. Bursts of the smallest particles at the lowest detectable sizes ( $\sim 2.5\ nm$ ) were  
237 not observed; however, we hypothesize that, during the NPF event, particle formation occurred

238 elsewhere and that subsequent horizontal extension caused the particles to reach the sampling site.  
239 Previously, NPF events have been identified on the regional scale in several locations around the world  
240 (Kerminen et al., 2018; Németh and Salma, 2014; Tremblay et al., 2019; Vana et al., 2004; Väänänen et  
241 al., 2013). For instances, Németh and Salma (2014) found that a nucleating air mass in regional NPF  
242 events may originate horizontally as far as several hundreds of kilometers (~400 or 700 km) away from  
243 the sampling site. Tremblay et al (2019) also concluded that particle nucleation events occurred over  
244 spatial scales of at least 500 km during the summertime in the Canadian High Arctic. In this section,  
245 case studies are discussed, including (i) marine Arctic NPF event, (ii) terrestrial Arctic NPF event, and  
246 (iii) pacific marine aerosol categories. During these temporal periods, the influences of the origins and  
247 pathways of air masses on the characteristics of particle formation and growth were investigated.

### 248 249 **3.2.1. Open ocean marine Arctic NPF event case study**

250 The marine Arctic NPF event was observed on September 3, 2017, and time series plots of the  
251 particle size distribution and air mass origins are presented in Fig. 4.  $N_{\text{NUC}}$  increased from  $77 \text{ cm}^{-3}$  to  
252  $757 \text{ cm}^{-3}$ , while  $N_{\text{AIT}}$  varied little. The elevated number concentration of nucleation-mode particles  
253 lasted for over five hours and then disappeared. Geometric mean diameter (GMD) varied from 14.6 to  
254 18.2 nm with an average of 16.3 nm, indicating that particle growth hardly occurred. The GMD is  
255 defined as the particle diameter at which the cumulative probability becomes 50% for the fitted log-  
256 normal distribution (Hinds, 1999). During the day, air masses traveled over the Arctic Ocean (explicitly,  
257 47.6, 0 and 0.4 h over the Arctic Ocean, Pacific Ocean and land domain, respectively), and have been  
258 categorized as Arctic Ocean originated air masses. As shown in Fig. S1, the satellite-derived  
259 chlorophyll-*a* concentration indicated a relatively high level of biological activity in the ocean during  
260 the time period focused upon in this study. It was noteworthy that the monthly mean chlorophyll  
261 concentration in the Beaufort and Chukchi Seas ( $2.24 \pm 3.44 \text{ mg m}^{-3}$ ;  $65^{\circ}\text{N}$ – $74^{\circ}\text{N}$  and  $170^{\circ}\text{E}$ – $120^{\circ}\text{W}$ )  
262 was approximately 3-fold greater than that estimated in the Pacific Ocean including the Bering Sea and  
263 the Sea of Okhotsk ( $0.83 \pm 1.30 \text{ mg m}^{-3}$ ;  $40^{\circ}\text{N}$ – $65^{\circ}\text{N}$  and  $145^{\circ}\text{E}$ – $168^{\circ}\text{W}$ ) (Fig. S1). Moreover, the

264 marginal ice zone is commonly associated with intense algae blooms during the melting season,  
265 therefore, significant emissions of biogenic trace gases such as DMS have been detected in the sea-ice  
266 edge (Levasseur, 2013; Oziel et al., 2017). Accordingly, as our measurements were collected over the  
267 Arctic Ocean onboard the ice breaker, marine biogenic sources could be considered as an important  
268 factor inducing NPF events.

269 Fig. 4d shows cosine of the solar zenith angle ( $\cos(\text{SZA})$ ) data that can be used as a proxy for solar  
270 energy reaching the ground surface. In addition, cloudiness which usually affects the real solar radiation  
271 reaching the surface was compared based on Moderate Resolution Imaging Spectroradiometer  
272 (MODIS) cloud fraction retrievals (Fig. S5). The data showed that cloud fraction was significantly high  
273 during the entire sampling periods, in general agreement with some other studies over the western  
274 Arctic region (e.g., Dong et al., 2010; Collines et al., 2017). In detail, the cloud fraction was relatively  
275 low for week 1 (8/29/2017–9/5/2017; Fig. S5a) and week 3 (9/14/2017–9/21/2017; Fig. S5c) when  
276 NPF event and growth was frequently observed (Fig. 3). This suggests that solar radiation at the surface,  
277 which is affected both by the cloud cover and SZA, may have influenced aerosol concentration and NPF  
278 observed here. As illustrated in Fig 4, the NPF event occurred when the sun was below the horizon (i.e.,  
279 Arctic nighttime nucleation). Typically, nucleation tends to take place preferably with high solar  
280 irradiation during the daytime (Kulmala et al., 2004). In several locations, however, also nighttime  
281 nucleation has been observed at Tumbarumba in Australian (Sunı et al., 2008), at Värriö measurement  
282 station in Finnish Lapland (Vehkamäki et al., 2004), and at a subarctic site in northern Sweden (~14 km  
283 east of Abisko) (Svenningsson et al., 2008). The possible explanation for nighttime events is that the  
284 actual formation and growth occurred even during daylight, but very slow growth in the Arctic and  
285 marine atmosphere allowed to detect the particles (~ 8 nm) only after sunset (Vehkamäki et al., 2004).  
286 Previous study reported that 32% of strong nighttime nucleation events (2.5 times as frequent as  
287 daytime nucleation event) were appeared in the presence of a very efficient ion source such as the  
288 strong radon efflux from the Tumbarumba soil (Sunı et al., 2008). Due to their rarity, the major  
289 mechanisms for nocturnal aerosol production are still unclear and require more study.

290

### 291 **3.2.2. Open ocean terrestrial Arctic NPF event case study**

292 The terrestrial Arctic NPF event was observed during September 13–14 2017. As shown in Fig. 5,  
293 significant strong NPF events occurred frequently during this period. The number concentration of total  
294 particles increased considerably, as a  $CN_{2.5}$  value exceeding  $\sim 6016 \text{ cm}^{-3}$  was observed during this event.  
295 In addition, the average concentrations of  $N_{\text{NUC}}$  and  $N_{\text{AIT}}$  during the terrestrial Arctic NPF were  $931 \pm$   
296  $222$  and  $1127 \pm 380 \text{ cm}^{-3}$ , respectively. This indicates that high  $CN_{2.5}$  concentration mainly contributed  
297 by nucleation and Aitken-mode particles (45 and 54% of the size distribution for nucleation-mode and  
298 Aitken-mode particles, respectively). GMD increased from 13.9 to 33.3 nm, indicating that the  
299 nucleation-mode particles subsequently increased in size. The formation and growth of aerosol particles  
300 were observed during the daytime (Fig. 5d), suggesting that photochemistry is involved. [During this](#)  
301 [period, air masses were heavily influenced by northern Alaska.](#) The average retention times of the 2-day  
302 back trajectories arriving at the ship position over the northern Alaska, Arctic Ocean and Pacific Ocean  
303 were 40.8, 7.2 and 0 h, respectively (Fig. 5e). It can be seen that the photochemical reactions of  
304 precursor gases (e.g., volatile organic compounds (VOCs) such as isoprene, monoterpenes, and  
305 sesquiterpenes) emitted by terrestrial ecosystems in Alaska were associated with new particle formation  
306 and growth (Schollert et al., 2014; TAPE et al., 2006; Kolesar et al., 2017; Ström et al., 2003).

307

### 308 **3.2.3. Pacific marine aerosol case study**

309 A typical aerosol scenario for Pacific marine air masses was observed on September 21–22, 2017,  
310 when the air masses passed over mainly the Pacific Ocean (including the Bering Sea and Sea of  
311 Okhotsk) (explicitly, 0, 47.9 and 0.1 h over the Arctic Ocean, Pacific Ocean and land domain,  
312 respectively) (Fig. 1a). As shown in Fig. 6, the aerosol number concentrations exhibited a bimodal size  
313 distribution, peaking at size ranges of 30 – 80 nm (Aitken mode) and 100 – 300 nm (accumulation  
314 mode), respectively. In contrast, the concentrations of nucleation-mode particles were very low. For  
315 example, the concentration of  $N_{\text{NUC}}$  ranged from 1 to  $38 \text{ cm}^{-3}$  with an average of  $8 \pm 4 \text{ cm}^{-3}$ . We also

316 observed CN<sub>2.5</sub> values at the background level of  $\sim 460 \pm 70 \text{ cm}^{-3}$ , which are consistent with the  
317 measurements collected at a coastal Antarctic station during summer ( $\sim 600 \text{ cm}^{-3}$ ) (Kim et al., 2017) and  
318 from flight-based measurements over the Arctic Ocean ( $\sim 300 \text{ cm}^{-3}$ ) (Burkart et al., 2017a).

319

### 320 **3.3. Overview of aerosol properties according to different air mass back trajectories**

321 Air masses comprising marine Pacific along with marine and terrestrial Arctic air masses were  
322 encountered during the campaign. In the section 3.2, two case studies of NPF events (Fig. 4 and Fig. 5)  
323 were found in the Arctic atmosphere. As stressed in Willis et al., (2018), NPF and growth is frequently  
324 observed in the boundary layer in the both Arctic open ocean and coastal regions. These events seem to  
325 occur more frequently than lower-latitude marine boundary layers (Quinn and Bates, 2011); there are  
326 multiple reasons including summer 24-h high solar radiation, low condensation sink, low temperature  
327 and low mixing of surface emissions, as recently reviewed in Abbatt et al. (2019). Our study also  
328 confirmed that any NPF was not detected during the Pacific transect.

329 In this section, we present an overall meteorological air mass summary of the open ocean field study,  
330 categorizing it into three synoptic period types: Pacific marine, Arctic marine and Arctic terrestrial.  
331 These classifications do not represent specific air mass back trajectories analysis, but they can mainly  
332 represent air masses that have been travelled over these three distinct geographical regions (section 2.4).  
333 Average size distributions for the three selected periods in the different air masses are shown in Fig. 7.  
334 To obtain the number size distribution in the size range from 7 nm to 300 nm as shown in Fig. 7, we  
335 used nano SMPS data from 7 nm to 64 nm and standard SMPS data from 64 nm to 300 nm. The nano  
336 SMPS and standard SMPS data agreed within  $\sim 8.8\%$  in their overlapping size range (10 – 64 nm) (Fig.  
337 S4), similar to a previous study (Watson et al., 2011). In addition, a summary of total number  
338 concentrations of particles for these periods is included in Table 1.

339

340 - *Arctic Marine*. A trimodal distribution was seen at  $18 \pm 3 \text{ nm}$ ,  $53 \pm 6 \text{ nm}$  and  $150 \pm 6 \text{ nm}$ . The first  
341 mode is due to NPF arriving from open pack sea ice and open ocean Arctic regions, as discussed in

342 Section 3.2.1 where a case study is presented. The Aitken mode (~53 nm) is remarkably similar to the  
343 Pacific Ocean aerosol size distribution and to previous studies detected in the Arctic regions (Tunved et  
344 al., 2013; Freud et al., 2017; Dall'Osto et al., 2019). The largest mode at ~150 nm may be due to a  
345 combination of primary and secondary aerosol components.

346  
347 - *Arctic terrestrial*. A bimodal distribution is seen with two main modes at  $24 \pm 3$  nm and  $151 \pm 3$  nm,  
348 respectively. The nucleation and Aitken modes are much higher than the accumulation mode, suggesting  
349 that NPF governs the aerosol processes in this coastal region at this time of the year.

350  
351 - *Pacific marine*. The Pacific Ocean aerosol size distributions showed a trimodal size distribution at  $56$   
352  $\pm 3$  nm,  $130 \pm 3$  nm and  $220 \pm 6$  nm. The lowest peak at ~56 nm (i.e., Aitken mode) is likely a  
353 combination of primary and secondary marine aerosol components, whereas the largest peak at ~220  
354 nm might be caused by cloud processing and aged aerosols. The mode at ~130 nm could originate from  
355 primary sea spray aerosols in the Pacific atmosphere (Quinn et al., 2015). When the distribution is fitted  
356 with log-normal modes, the inter-modal minimum is calculated to be ~120 nm - often known as Hoppel  
357 minimum as a signature of cloud processing (Hoppel et al., 1994) - although, it is difficult to draw a  
358 firm conclusion due to the overlap with the third mode at ~130 nm.

359  
360 This study shows that aerosol originating from higher and lower marine latitudes – although both  
361 being treated as marine air masses - have very different features, as pointed out in several previous  
362 studies (Dall'Osto et al., 2010; Frossard et al., 2014). A key conclusion of this study is that we also need  
363 to separate different bioregions in the Arctic, especially given the current results showing very different  
364 aerosol size distributions in the Arctic study areas (Fig. 7; Arctic marine and Arctic terrestrial). The  
365 reasons for the much higher aerosol concentrations near the coast of Alaska relative to the open ocean  
366 sympagic and pelagic regions may be multiple. We discuss at least two major sources may contribute to  
367 the high aerosol concentrations recorded.

368 The first source of aerosols in the [late summer](#) terrestrial Arctic air masses may be due to

369 anthropogenic sources. Due to sea ice retreat and better technologies, the Arctic is now easily accessible  
370 to human activities, including oil and gas extraction (Law and Stohl, 2007; Peters et al., 2011). These  
371 Arctic oil fields can emit the large amounts of aerosols, and with on-going Arctic development, such  
372 local combustion emissions may increase in the future, possibly affecting local air quality (Gunsch et al.,  
373 2017; Schmale et al., 2018a). In fact, some NPF events were reported within the North Slope of Alaska  
374 (e.g., Prudhoe Bay oil fields) during August and September 2016 at Oliktok Point Alaska. This  
375 observation was suggested to be linked with oil fields emissions (Kolesar et al., 2017). However, our  
376 measurements were conducted in the open ocean, quite far from any land oil field local emissions. BC  
377 data were collected as shown in Fig. 8; they revealed very high standard deviations due to high  
378 detection limit of the instrument used relative to the concentrations detected. However, no remarkable  
379 differences can be seen, all pointing to pristine clean marine air masses with BC values of  
380 approximately  $20 \pm 10 \text{ ng m}^{-3}$ . The two Arctic categories (Marine and Terrestrial) shows similar BC  
381 values, whereas higher values can be seen for the Pacific marine aerosol category, probably due to  
382 contamination from nearby Asian high pollutant sources.

383 The second source of aerosol in the [late summer](#) terrestrial Arctic air masses may be due to terrestrial  
384 natural sources. We believe that this may be a much more probable reason. The Arctic Ocean is  
385 submerged under areas of relatively shallow water known as a shelf sea for ~50% of its area. It is a  
386 relatively small ocean, characterized by pronounced riverine influence and a complex hydrography. Up  
387 to 11% of the entire global river discharge ends up in the Arctic Ocean (Shiklomanov et al., 2000),  
388 which is only 1% of the global ocean volume. The discharge of freshwater is increasing (Peterson et al.,  
389 2002), impacting coastal salinity and carbon cycle. Indeed, this continental runoff is a major source of  
390 freshwater, nutrients and terrigenous material to the Arctic Ocean (Benner et al., 2005; Fichot et al.,  
391 2013; Massicotte et al., 2017). The warming climate in the region is causing permafrost degradation,  
392 alterations to regional hydrology and shifting amounts and composition of dissolved organic matter  
393 (DOM) transported by streams and rivers (Mann et al., 2016; Chen et al., 2017). Overall, there is a  
394 considerable spatial and temporal heterogeneity in the distribution of the DOC in the Arctic, owing to

395 strong biological and physicochemical processes. It is important to remember that sea ice formation and  
396 melting also affects the concentrations and distributions of DOC, although its impact is still difficult to  
397 resolve (Fichot et al., 2013; Shen et al., 2012).

398 In a recent paper (Park et al., 2019), we suggested that the large amount of freshwater from river  
399 runoff may have a substantial impact on primary aerosol production mechanisms, possibly affecting the  
400 cloud radiative forcing. We showed that the Arctic riverine organic matter can be directly emitted from  
401 surface seawater into the atmosphere via bubble bursting (Park et al., 2019). The high amount of DOC  
402 populating the sea-surface microlayer (SML) in the Arctic waters - including UV absorbing humic  
403 substances - can also produce VOCs (Ciuraru et al., 2015; Fu et al., 2015), which are known precursors  
404 of secondary organic aerosols. Recently, Mungall et al. (2017) reported that the marine microlayer in the  
405 Canadian Arctic Archipelago is a source of oxidized VOCs (OVOCs), which could be an important  
406 source of biogenic secondary organic aerosol (Croft et al., 2019). Previous studies also reported  
407 fluorescent water-soluble organic aerosols in the High Arctic atmosphere (Fu et al., 2015). It is worth  
408 noting that terrestrial VOCs from tundra and lakes at elevated concentrations were reported (Potosnak et  
409 al., 2013; Lindwall et al., 2016; Steinke et al., 2018).

410 Fig. 9 shows DOC concentrations from water samples taken in the areas where the NPF marine and  
411 terrestrial case studies (Section 3.2.1 and 3.2.2) were detected. It is clear that as much as twice higher  
412 concentrations are seen for the coastal marine areas, relative to the open ocean marine regions. The  
413 origin of this organic matter can be obtained by the FDOM analysis. Fig. 9 (bottom) shows specific  
414 peaks attributed to different chemical features. The ratio of terrestrial humic substances (peak A) was  
415 3.5 for the terrestrial/marine samples. By striking contrast, marine fulvic substances (peak M) and  
416 proteinaceous (peak T) had a ratio of 0.45 and 0.27, respectively, showing two very distinct chemical  
417 compounds. This suggests that coastal oceanic water enriched in river organic material as well as fresh  
418 water tundra and lake may be a source of VOC (both from biotic and abiotic emission processes) that  
419 may be responsible for the high secondary aerosols detected near these areas.

420

### 3.4. Particle growth rates and condensation sink

Table 1 shows particle growth rate (GR) and condensation sink (CS) for Arctic marine, Arctic terrestrial and Pacific marine air masses. The GR was calculated by fitting a linear regression to the peak diameter of the aerosol size distribution for the nucleation-mode between 4 and 20 nm against time during the NPF cases (Dal Maso et al., 2005; Pierce et al., 2014). The GR observed during the Arctic marine and Arctic terrestrial air masses were the  $0.4 \pm 0.3 \text{ nm h}^{-1}$  and  $0.8 \pm 0.2 \text{ nm h}^{-1}$ , respectively, which was similar to the values previously observed from other Arctic regions. A shipboard expedition conducted during the summers of 2014 and 2016 throughout the Canadian Arctic, indicated that the GR varied widely from 0.2 to  $15.3 \text{ nm h}^{-1}$  (Collins et al., 2017). The GR observed at Summit, Greenland was  $0.2 \pm 0.1 \text{ nm h}^{-1}$  (range of 0.09 to  $0.3 \text{ nm h}^{-1}$ ) (Ziemba et al., 2010). Similarly, in Utqiagivik (Barrow), Alaska, the GR was  $1.0 \text{ nm h}^{-1}$  in air mass influenced by Beaufort Sea, whereas the value was  $11.1 \text{ nm h}^{-1}$  in air mass influenced by Prudhoe Bay (i.e., oil field area) (Kolesar et al., 2017). Particularly, simultaneous growth of multiple modes was present in some cases (9/13/2017– 9/21/2017). We calculated the GR of the distinct modes, as shown in Fig. S6. The results showed that growth of the larger mode (e.g., preexisting mode) was faster than the smaller mode (e.g., nucleation mode), consistent with ship-based aerosol measurements in the summertime Arctic by Burkart et al. (2017b). They proposed that growth was largely via condensation of semi-volatile organic material, because lower volatile organics could lead to faster growth of the smaller mode.

The CS is a key parameter assessing the NPF and growth and determines how rapidly gaseous molecules condense onto pre-existing particles. The CS was calculated, following Dal Maso et al. (2002) and Collines et al. (2017). The resulting CS values are given in Table 1. The CS observed during the Arctic marine and Arctic terrestrial air masses were  $0.5 \pm 0.4 \text{ nm h}^{-1}$  and  $0.9 \pm 0.5 \text{ nm h}^{-1}$ , respectively. The CS in this study is on the low end of the values observed during the summer in Arctic marine boundary layer (shipborne expeditions) (Collins et al., 2017), Utqiagivik, Alaska (Kolesar et al., 2017), and Ny-Ålesund, Svalbard (Giamarelou et al., 2016). In case when air mass passed over the Pacific Ocean, the CS was 2 or 4 times higher than those of Arctic air masses. It seems that such higher

447 CS for Pacific marine air masses lowered the concentration of condensable vapors, thereby resulting in  
448 the non-event days in Pacific marine air masses.

### 449 3.5. Impact on CCN number concentrations

450 Fig. 10a illustrates the CCN concentrations for the three selected periods under different  
451 supersaturation conditions. For a given SS of 0.4%, CCN concentrations for Arctic marine, Arctic  
452 terrestrial and Pacific marine air masses were  $35 \pm 40 \text{ cm}^{-3}$ ,  $71 \pm 47 \text{ cm}^{-3}$ , and  $204 \pm 87 \text{ cm}^{-3}$ ,  
453 respectively. Higher concentrations of CCN were observed when the air mass originated from the  
454 Pacific marine for a SS of 0.2%–1.0 %. This may have occurred due to the differences in the CCN  
455 sources between the Arctic and Pacific Oceans. It was noted that that accumulation and coarse-mode  
456 particles, which are predominant over the Pacific Ocean (Fig. 7), can easily act as CCN. Our results  
457 agreed well with values reported in previous studies that measured CCN at a ground-based Arctic  
458 station (Jung et al., 2018), but was slightly higher than those measured from high-Arctic expeditions  
459 (Leck et al., 2002; Martin et al., 2011; Mauritsen et al., 2011). For example, Jung et al. (2018) reported  
460 seasonal variations in the CCN concentration over seven years (2007–2013) at the Zeppelin station, and  
461 found that the monthly mean CCN concentrations ranged from  $17 \text{ cm}^{-3}$  in October 2007 to  $198 \text{ cm}^{-3}$  in  
462 March 2008 at a SS value of 0.4%. However, Mauritsen et al. (2011) observed CCN concentrations  
463 lower than  $\sim 100 \text{ cm}^{-3}$  at five different supersaturations (SS = 0.10%, 0.15%, 0.20%, 0.41%, and 0.73%),  
464 with median values ranging from 15 to  $50 \text{ cm}^{-3}$ , in four High Arctic expeditions during the Arctic  
465 Summer Cloud Ocean Study. Such values were also in line with the long term measurement at an Arctic  
466 station in Barrow, which indicated that the median CCN concentrations at 0.2% SS was smaller than  
467  $100 \text{ cm}^{-3}$  (Schmale et al., 2018b).

468 We also compared CCN activity and critical diameter for the three selected periods, as shown in Fig.  
469 10b and c. The CCN activity is defined as the ratio of the number concentration of particles that  
470 activated to become CCN at a given supersaturation to the total number concentration of particles larger  
471 than 2.5nm ( $\text{CN}_{2.5}$ ). The CCN activity followed a similar pattern as the CCN concentration.  
472 Furthermore, the critical diameter ( $D_c$ ) (i.e., the diameter at which the integration of aerosol size

473 distribution from the largest particle diameter to the lower ones matches with the measured CCN  
474 concentration) was estimated using the measured aerosol size distribution,  $CN_{2.5}$ , and CCN  
475 concentrations with a time resolution of 1 h, as described by Furutani et al., (2014). The  $D_c$  at a SS of  
476 0.4% was found to be  $103 \pm 43$  nm,  $83 \pm 18$  nm, and  $136 \pm 67$  nm for Arctic marine, Arctic terrestrial,  
477 and Pacific marine periods, respectively. These values are comparable to previous studies obtained in  
478 the Arctic and subarctic regions. For instance, the  $D_c$  of 80 nm at 0.6 % SS was observed during the  
479 aircraft measurement in July 2014 in the high Arctic marine boundary layer of Resolute Bay, Nunavut,  
480 Canada (Burkart et al., 2017a). Jaatinen et al. (2014) reported that the  $D_c$  value of  $98 \pm 16$  nm (SS =  
481 0.4%) from the subarctic area of Finland (Pallas-Sodankylä Global Atmospheric Watch station). Anttila  
482 et al. (2012) also showed that a  $D_c$  value was in the range of 90 to 120 nm at a SS of 0.4% during the  
483 same field campaign as reported in Jaatinen et al. (2014). For a maximum SS between 0.18 and 0.26%,  
484  $D_c$  varied between 110 and 140 nm at the same measurement sites.

#### 485 486 **4. Summary and conclusions**

487 This study presents the physical properties of aerosol particles measured aboard the R/V Araon ice-  
488 breaker during 2017 throughout the Arctic and Pacific Oceans. The  $CN_{2.5}$  value commonly ranged  
489 between 13 and 2000  $cm^{-3}$  with an average of  $505 \pm 280$   $cm^{-3}$ . An elevated  $CN_{2.5}$  concentration reaching  
490  $\sim 6016$   $cm^{-3}$  was observed from 13 September to 20 September. The temporal variations in the  $CN_{2.5}$   
491 concentration followed a similar pattern to those of  $N_{NUA}$  and  $N_{AIT}$ . We also found that the  $CN_{2.5}$   
492 concentration was strongly correlated with  $N_{NUA}$  ( $r^2 = 0.69$ ), suggesting that CN was mainly derived  
493 from nucleation-mode particles.

494 NPF events caused by gas-to-particle conversion frequently occurred over the Arctic Ocean.  
495 Overall, two major NPF sources (i.e., Arctic marine and Arctic terrestrial) were identified based on the  
496 backward air mass trajectory analysis. NPF events were associated with Arctic marine air masses,  
497 indicating the impact of marine biogenic emissions from the Arctic Ocean. Strong NPF events with  
498 particle growth were associated with Arctic terrestrial air masses, which may be due to the biogenic

499 precursor gases emitted by terrestrial ecosystems including river discharge and Alaskan tundra in the  
500 Arctic coastal areas. In contrast, relatively larger particles with broad Aitken and accumulation-mode  
501 peaks were observed over the Pacific Ocean. Our study confirmed that any NPF was not detected during  
502 the Pacific transect. We also compared the average CCN concentrations for each of the cases. Our data  
503 showed that the impact of aerosols on CCN concentrations ( $SS = 0.4\%$ ) was significant:  $35 \pm 40 \text{ cm}^{-3}$ ,  
504  $71 \pm 47 \text{ cm}^{-3}$ , and  $204 \pm 87 \text{ cm}^{-3}$  for Arctic marine, Arctic terrestrial, and Pacific marine periods,  
505 respectively. Our interpreted data showed that river outflows and tundra strongly influence Arctic  
506 aerosol properties. Further detailed measurements of the chemical characteristics of marine aerosols are  
507 required to provide more direct evidence for the contribution of biogenic precursors to the NPF and  
508 CCN in the remote Arctic atmosphere.

509 Arctic areas are currently experiencing drastic climate change, with air temperatures increasing at  
510 twice the rate of the global average. This warming is causing clear changes, such as the increases in  
511 biogenic emissions from tundra vegetation and changes in vegetation cover (Faubert et al., 2010;  
512 Peñuelas and Staudt, 2010; Potosnak et al., 2013; Lindwall et al., 2016). Lindwall et al. (2016) observed  
513 a 280% increase in VOC emissions relative to the ambient level in response to a  $4 \text{ }^\circ\text{C}$  increase in the  
514 summer temperature of the Subarctic. Increases in VOC emissions from river discharge and tundra  
515 vegetation in the Arctic are critical factors that induce NPF and particle growth events, which may  
516 impact the CCN concentrations during the Arctic summer.

#### 517 518 **Data availability**

519 The data analyzed in this publication will be readily provided upon request to the corresponding author  
520 (yjyoon@kopri.re.kr).

#### 521 522 **Author contributions**

523 JP, YJY designed the study, JP, MD'O, KP, YG, HJK, EJ, KTP, MP, SSY, JJ, and BYL analyzed data.  
524 JP, MD'O, KTP and YJY prepared the manuscript with contributions from all co-authors.

#### 525 526 **Competing interests**

527 The authors declare that they have no conflict of interest.

528

529 **Acknowledgements**

530 We are grateful to the captain and crews of R/V *Araon* for their enthusiastic assistance during the cruise  
 531 of ARA08C. This work was supported by a Korea Grant from the Korean Government (MSIP) (NRF-  
 532 2016M1A5A1901769) (KOPRI-PN20081) and the KOPRI projects (PE17390 and [PE20060](#)). Kihong  
 533 Park was supported by the National Leading Research Laboratory program (NRF-2019R1A2C3007202).  
 534 Minsu Park and Seong Soo Yum were supported by National Research Foundation of Korea (NRF)  
 535 grant (NRF-20180R1A2B2006965). Jinyoung Jung was supported by “Korea-Arctic Ocean Observing  
 536 System (K-AOOS)”, KOPRI, 20160245, funded by the MOF, Korea.

537

538 **References**

- 539 Abbatt, J. P. D., Leaitch, W. R., Aliabadi, A. A., Bertram, A. K., Blanchet, J. P., Boivin-Rioux, A.,  
 540 Bozem, H., Burkart, J., Chang, R. Y. W., Charette, J., Chaubey, J. P., Christensen, R. J., Cirisan,  
 541 A., Collins, D. B., Croft, B., Dionne, J., Evans, G. J., Fletcher, C. G., Galí, M.,  
 542 Ghahremaninezhad, R., Girard, E., Gong, W., Gosselin, M., Gourdal, M., Hanna, S. J.,  
 543 Hayashida, H., Herber, A. B., Hesaraki, S., Hoor, P., Huang, L., Husserr, R., Irish, V. E., Keita,  
 544 S. A., Kodros, J. K., Köllner, F., Kolonjari, F., Kunkel, D., Ladino, L. A., Law, K., Levasseur, M.,  
 545 Libois, Q., Liggio, J., Lizotte, M., Macdonald, K. M., Mahmood, R., Martin, R. V., Mason, R. H.,  
 546 Miller, L. A., Moravek, A., Mortenson, E., Mungall, E. L., Murphy, J. G., Namazi, M., Norman,  
 547 A. L., O'Neill, N. T., Pierce, J. R., Russell, L. M., Schneider, J., Schulz, H., Sharma, S., Si, M.,  
 548 Staebler, R. M., Steiner, N. S., Thomas, J. L., von Salzen, K., Wentzell, J. J. B., Willis, M. D.,  
 549 Wentworth, G. R., Xu, J. W., and Yakobi-Hancock, J. D.: Overview paper: New insights into  
 550 aerosol and climate in the Arctic, *Atmos. Chem. Phys.*, 19, 2527-2560, 10.5194/acp-19-2527-  
 551 2019, 2019.
- 552 ACIA: Arctic Climate Impact Assessment, chap. 2, p. 23, Cambridge University Press, New York, USA,,  
 553 2005.
- 554 Allan, J. D., Williams, P. I., Najera, J., Whitehead, J. D., Flynn, M. J., Taylor, J. W., Liu, D., Darbyshire,  
 555 E., Carpenter, L. J., Chance, R., Andrews, S. J., Hackenberg, S. C., and McFiggans, G.: Iodine  
 556 observed in new particle formation events in the Arctic atmosphere during ACCACIA, *Atmos.*  
 557 *Chem. Phys.*, 15, 5599-5609, 10.5194/acp-15-5599-2015, 2015.
- 558 Asmi, E., Kondratyev, V., Brus, D., Laurila, T., Lihavainen, H., Backman, J., Vakkari, V., Aurela, M.,  
 559 Hatakka, J., Viisanen, Y., Uttal, T., Ivakhov, V., and Makshtas, A.: Aerosol size distribution  
 560 seasonal characteristics measured in Tiksi, Russian Arctic, *Atmos. Chem. Phys.*, 16, 1271-1287,  
 561 10.5194/acp-16-1271-2016, 2016.
- 562 Benner, R., Louchouart, P., and Amon, R. M. W.: Terrigenous dissolved organic matter in the Arctic  
 563 Ocean and its transport to surface and deep waters of the North Atlantic, *Global Biogeochemical*  
 564 *Cycles*, 19, doi:10.1029/2004GB002398, 2005.
- 565 Burkart, J., Willis, M. D., Bozem, H., Thomas, J. L., Law, K., Hoor, P., Aliabadi, A. A., Köllner, F.,  
 566 Schneider, J., Herber, A., Abbatt, J. P. D., and Leaitch, W. R.: Summertime observations of  
 567 elevated levels of ultrafine particles in the high Arctic marine boundary layer, *Atmos. Chem.*  
 568 *Phys.*, 17, 5515-5535, 10.5194/acp-17-5515-2017, 2017a.

- 569 Burkart, J., Hodshire, A. L., Mungall, E. L., Pierce, J. R., Collins, D. B., Ladino, L. A., Lee, A. K. Y.,  
570 Irish, V., Wentzell, J. J. B., Liggio, J., Papakyriakou, T., Murphy, J., Abbatt, J.: Organic  
571 condensation and particle growth to CCN sizes in the summertime marine Arctic is driven by  
572 materials more semivolatile than at continental sites, *Geophys. Res. Lett.* 44, 10725–10734.  
573 <https://doi.org/10.1002/2017GL075671>, 2017 b.
- 574 Chang, R. Y.-W., Sjostedt, S. J., Pierce, J. R., Papakyriakou, T. N., Scarratt, M. G., Michaud, S.,  
575 Levasseur, M., Leaitch, W. R., and Abbatt, J. P. D.: Relating atmospheric and oceanic DMS  
576 levels to particle nucleation events in the Canadian Arctic, *Journal of Geophysical Research:*  
577 *Atmospheres*, 116, doi:10.1029/2011JD015926, 2011.
- 578 Chen, X., Zhang, X., Church, J. A., Watson, C. S., King, M. A., Monselesan, D., Legresy, B., and Harig,  
579 C.: The increasing rate of global mean sea-level rise during 1993–2014, *Nature Climate Change*,  
580 7, 492, 10.1038/nclimate3325 [https://www.nature.com/articles/nclimate3325#supplementary-](https://www.nature.com/articles/nclimate3325#supplementary-information)  
581 [information](https://www.nature.com/articles/nclimate3325#supplementary-information), 2017.
- 582 Ciuraru, R., Fine, L., van Pinxteren, M., D'Anna, B., Herrmann, H., and George, C.: Photosensitized  
583 production of functionalized and unsaturated organic compounds at the air-sea interface,  
584 *Scientific Reports*, 5, 12741, 10.1038/srep12741 [https://www.nature.com/articles/srep12741](https://www.nature.com/articles/srep12741#supplementary-information)  
585 [#supplementary-information](https://www.nature.com/articles/srep12741#supplementary-information), 2015.
- 586 Coble, P. G.: Marine Optical Biogeochemistry: The Chemistry of Ocean Color, *Chemical Reviews*, 107,  
587 402-418, 10.1021/cr050350+, 2007.
- 588 Collins, D. B., Burkart, J., Chang, R. Y.-W., Lizotte, M., Boivin-Rioux, A., Blais, M., Mungall, E. L.,  
589 Boyer, M., Irish, V. E., Massé, G., Kunkel, D., Tremblay, J.-É., Papakyriakou, T., Bertram, A. K.,  
590 Bozem, H., Gosselin, M., Levasseur, M., and Abbatt, J. P. D.: Frequent ultrafine particle  
591 formation and growth in Canadian Arctic marine and coastal environments, *Atmos. Chem. Phys.*,  
592 17, 13119–13138, <https://doi.org/10.5194/acp-17-13119-2017>, 2017.
- 593 Croft, B., Martin, R. V., Leaitch, W. R., Tunved, P., Breider, T. J., D'Andrea, S. D., and Pierce, J. R.:  
594 Processes controlling the annual cycle of Arctic aerosol number and size distributions, *Atmos.*  
595 *Chem. Phys.*, 16, 3665-3682, 10.5194/acp-16-3665-2016, 2016.
- 596 Croft, B., Martin, R. V., Leaitch, W. R., Burkart, J., Chang, R. Y. W., Collins, D. B., Hayes, P. L.,  
597 Hodshire, A. L., Huang, L., Kodros, J. K., Moravek, A., Mungall, E. L., Murphy, J. G., Sharma,  
598 S., Tremblay, S., Wentworth, G. R., Willis, M. D., Abbatt, J. P. D., and Pierce, J. R.: Arctic  
599 marine secondary organic aerosol contributes significantly to summertime particle size  
600 distributions in the Canadian Arctic Archipelago, *Atmos. Chem. Phys.*, 19, 2787-2812,  
601 10.5194/acp-19-2787-2019, 2019.
- 602 Dall'Osto, M., Ceburnis, D., Martucci, G., Bialek, J., Dupuy, R., Jennings, S. G., Berresheim, H.,  
603 Wenger, J., Healy, R., Facchini, M. C., Rinaldi, M., Giulianelli, L., Finessi, E., Worsnop, D., Ehn,  
604 M., Mikkilä, J., Kulmala, M., and O'Dowd, C. D.: Aerosol properties associated with air masses  
605 arriving into the North East Atlantic during the 2008 Mace Head EUCAARI intensive observing  
606 period: an overview, *Atmos. Chem. Phys.*, 10, 8413-8435, 10.5194/acp-10-8413-2010, 2010.
- 607 Dall'Osto, M., Beddows, D. C. S., Tunved, P., Harrison, R. M., Lupi, A., Vitale, V., Becagli, S., Traversi,  
608 R., Park, K. T., Yoon, Y. J., Massling, A., Skov, H., Lange, R., Strom, J., and Krejci, R.:  
609 Simultaneous measurements of aerosol size distributions at three sites in the European high  
610 Arctic, *Atmos. Chem. Phys.*, 19, 7377-7395, 10.5194/acp-19-7377-2019, 2019.
- 611 Dall'Osto, M., Beddows, D. C. S., Tunved, P., Krejci, R., Ström, J., Hansson, H. C., Yoon, Y. J., Park,  
612 K.-T., Becagli, S., Udisti, R., Onasch, T., O'Dowd, C. D., Simó, R., and Harrison, R. M.: Arctic  
613 sea ice melt leads to atmospheric new particle formation, *Scientific Reports*, 7, 3318,  
614 10.1038/s41598-017-03328-1, 2017.
- 615 Dal Maso, M.: Condensation and coagulation sinks and formation of nucleation mode particles in  
616 coastal and boreal forest boundary layers, *J. Geophys. Res.*, 107, 10.1029/2001jd001053, 2002.
- 617 Dal Maso, M., Kulmala, M., Riipinen, I., Wagner, R., Hussein, T., Aalto, P. P., and Lehtinen, K. E. J.:  
618 Formation and growth of fresh atmospheric aerosols: Eight years of aerosol size distribution data  
619 from SMEAR II, Hyytiälä, Finland, *Boreal Environment Research*, 10, 323-336, 2005.

620 Dong, X., Xi, B., Crosby, K., Long, C. N., Stone, R. S., and Shupe, M.: A 10 year climatology of Arctic  
621 cloud fraction and radiative forcing at Barrow, Alaska, *J Geophys Res-Atmos*, 115, D17212,  
622 [doi.org/10.1029/2009JD013489](https://doi.org/10.1029/2009JD013489), 2010.

623 Ehn, M., Vuollekoski, H., Petäjä, T., Kerminen, V.-M., Vana, M., Aalto, P., de Leeuw, G., Ceburnis, D.,  
624 Dupuy, R., O'Dowd, C. D., and Kulmala, M.: Growth rates during coastal and marine new  
625 particle formation in western Ireland, *J Geophys Res-Atmos*, 115, doi:10.1029/  
626 2010JD014292, 2010.

627 Faubert, P., Tiiva, P., Rinnan, Å., Michelsen, A., Holopainen, J. K., and Rinnan, R.: Doubled volatile  
628 organic compound emissions from subarctic tundra under simulated climate warming, 187, 199-  
629 208, [10.1111/j.1469-8137.2010.03270.x](https://doi.org/10.1111/j.1469-8137.2010.03270.x), 2010.

630 Fichot, C. G., Kaiser, K., Hooker, S. B., Amon, R. M. W., Babin, M., Bélanger, S., Walker, S. A., and  
631 Benner, R.: Pan-Arctic distributions of continental runoff in the Arctic Ocean, *Scientific Reports*,  
632 3, 1053, [10.1038/srep01053](https://doi.org/10.1038/srep01053) [https://www.nature.com/articles/srep01053#supplementary-](https://www.nature.com/articles/srep01053#supplementary-information)  
633 [information](https://www.nature.com/articles/srep01053#supplementary-information), 2013.

634 Freud, E., Krejci, R., Tunved, P., Leaitch, R., Nguyen, Q. T., Massling, A., Skov, H., and Barrie, L.:  
635 Pan-Arctic aerosol number size distributions: seasonality and transport patterns, *Atmos. Chem.*  
636 *Phys.*, 17, 8101-8128, [10.5194/acp-17-8101-2017](https://doi.org/10.5194/acp-17-8101-2017), 2017.

637 Frossard, A. A., Russell, L. M., Burrows, S. M., Elliott, S. M., Bates, T. S., and Quinn, P. K.: Sources  
638 and composition of submicron organic mass in marine aerosol particles, 119, 12,977-913,003,  
639 [10.1002/2014jd021913](https://doi.org/10.1002/2014jd021913), 2014.

640 Fu, P., Kawamura, K., Chen, J., Qin, M., Ren, L., Sun, Y., Wang, Z., Barrie, L. A., Tachibana, E., Ding,  
641 A., and Yamashita, Y.: Fluorescent water-soluble organic aerosols in the High Arctic atmosphere,  
642 *Scientific Reports*, 5, 9845, [10.1038/srep09845](https://doi.org/10.1038/srep09845), 2015.

643 Giamarelou, M., Eleftheriadis, K., Nyeki, S., Tunved, P., Torseth, K., and Biskos, G.: Indirect evidence  
644 of the composition of nucleation mode atmospheric particles in the high Arctic, *J. Geophys.*  
645 *Res.-Atmos.*, 121, 965–975, <https://doi.org/10.1002/2015JD023646>, 2016.

646 Gunsch, M. J., Kirpes, R. M., Kolesar, K. R., Barrett, T. E., China, S., Sheesley, R. J., Laskin, A.,  
647 Wiedensohler, A., Tuch, T., and Pratt, K. A.: Contributions of transported Prudhoe Bay oil field  
648 emissions to the aerosol population in Utqiagvik, Alaska, *Atmos. Chem. Phys.*, 17, 10879-10892,  
649 [10.5194/acp-17-10879-2017](https://doi.org/10.5194/acp-17-10879-2017), 2017.

650 Hinds, W. C.: *Aerosol Technology: Properties, Behavior, and Measurement of Airborne Particles, 2nd*  
651 *edn., Wiley-Interscience, New York, 1999.*

652 Heintzenberg, J., Leck, C., and Tunved, P.: Potential source regions and processes of aerosol in the  
653 summer Arctic, *Atmos. Chem. Phys.*, 15, 6487-6502, [10.5194/acp-15-6487-2015](https://doi.org/10.5194/acp-15-6487-2015), 2015.

654 Heintzenberg, J., Tunved, P., Galí, M., and Leck, C.: New particle formation in the Svalbard region  
655 2006–2015, *Atmos. Chem. Phys.*, 17, 6153-6175, [10.5194/acp-17-6153-2017](https://doi.org/10.5194/acp-17-6153-2017), 2017.

656 Hoppel, W. A., Frick, G. M., Fitzgerald, J. W., and Larson, R. E.: Marine boundary layer measurements  
657 of new particle formation and the effects nonprecipitating clouds have on aerosol size  
658 distribution, 99, 14443-14459, [10.1029/94jd00797](https://doi.org/10.1029/94jd00797), 1994.

659 Hudson, J. G., and Yum, S. S.: Cloud condensation nuclei spectra and polluted and clean clouds over the  
660 Indian Ocean, 107, INX2 21-21-INX22 21-12, [10.1029/2001jd000829](https://doi.org/10.1029/2001jd000829), 2002.

661 IPCC: *Climate change 2013: The physical science basis*, Intergovernmental panel on Climate Change,  
662 Cambridge University Press, New York, USA, 571-740, 2013.

663 Jang, E., Park, K. T., Yoon, Y. J., Kim, T. W., Hong, S. B., Becagli, S., Traversi, R., Kim, J., and Gim,  
664 Y.: New particle formation events observed at the King Sejong Station, Antarctic Peninsula –  
665 Part 2: Link with the oceanic biological activities, *Atmos. Chem. Phys.*, 19, 7595-7608,  
666 [10.5194/acp-19-7595-2019](https://doi.org/10.5194/acp-19-7595-2019), 2019.

667 Jung, C. H., Yoon, Y. J., Kang, H. J., Gim, Y., Lee, B. Y., Ström, J., Krejci, R., and Tunved, P.: The  
668 seasonal characteristics of cloud condensation nuclei (CCN) in the arctic lower troposphere,  
669 *Tellus B: Chemical and Physical Meteorology*, 70, 1-13, [10.1080/16000889.2018.1513291](https://doi.org/10.1080/16000889.2018.1513291), 2018.

670 Kalivitis, N., Kerminen, V. M., Kouvarakis, G., Stavroulas, I., Bougiatioti, A., Nenes, A., Manninen, H.

671 E., Petäjä, T., Kulmala, M., and Mihalopoulos, N.: Atmospheric new particle formation as a  
672 source of CCN in the eastern Mediterranean marine boundary layer, *Atmos. Chem. Phys.*, 15,  
673 9203-9215, 10.5194/acp-15-9203-2015, 2015.

674 Kerminen, V.-M., Chen, X., Vakkari, V., Petäjä, T., Kulmala, M., and Bianchi, F.: Atmospheric new  
675 particle formation and growth: review of field observations, *Environmental Research Letters*, 13,  
676 103003, 10.1088/1748-9326/aadf3c, 2018.

677 Kim, G., Cho, H.-j., Seo, A., Kim, D., Gim, Y., Lee, B. Y., Yoon, Y. J., and Park, K.: Comparison of  
678 Hygroscopicity, Volatility, and Mixing State of Submicrometer Particles between Cruises over  
679 the Arctic Ocean and the Pacific Ocean, *Environmental Science & Technology*, 49, 12024-12035,  
680 10.1021/acs.est.5b01505, 2015.

681 Kim, J., Yoon, Y. J., Gim, Y., Kang, H. J., Choi, J. H., Park, K. T., and Lee, B. Y.: Seasonal variations in  
682 physical characteristics of aerosol particles at the King Sejong Station, Antarctic Peninsula,  
683 *Atmos. Chem. Phys.*, 17, 12985-12999, 10.5194/acp-17-12985-2017, 2017.

684 Kim, J., Yoon, Y. J., Gim, Y., Choi, J. H., Kang, H. J., Park, K. T., Park, J., and Lee, B. Y.: New particle  
685 formation events observed at King Sejong Station, Antarctic Peninsula – Part 1: Physical  
686 characteristics and contribution to cloud condensation nuclei, *Atmos. Chem. Phys.*, 19, 7583-  
687 7594, 10.5194/acp-19-7583-2019, 2019.

688 Kolesar, K. R., Cellini, J., Peterson, P. K., Jefferson, A., Tuch, T., Birmili, W., Wiedensohler, A., and  
689 Pratt, K. A.: Effect of Prudhoe Bay emissions on atmospheric aerosol growth events observed in  
690 Utqiagvik (Barrow), Alaska, *Atmospheric Environment*, 152, 146-155,  
691 <https://doi.org/10.1016/j.atmosenv.2016.12.019>, 2017.

692 Kulmala, M., Vehkamäki, H., Petäjä, T., Dal Maso, M., Lauri, A., Kerminen, V. M., Birmili, W., and  
693 McMurry, P. H.: Formation and growth rates of ultrafine atmospheric particles: a review of  
694 observations, *Journal of Aerosol Science*, 35, 143-176,  
695 <https://doi.org/10.1016/j.jaerosci.2003.10.003>, 2004.

696 Law, K. S., and Stohl, A.: Arctic Air Pollution: Origins and Impacts, *Science*, 315, 1537-1540,  
697 10.1126/science.1137695, 2007.

698 Leaitch, W. R., Sharma, S., Huang, L., Toom-Saunty, D., Chivulescu, A., Macdonald, A. M., von  
699 Salzen, K., Pierce, J. R., Bertram, A. K., Schroder, J. C., Shantz, N. C., Chang, R. Y.-W., and  
700 Norman, A.-L.: Dimethyl sulfide control of the clean summertime Arctic aerosol and cloud,  
701 *Elem. Sci. Anth.*, 1, 000017, 10.12952/journal.elementa.000017, 2013.

702 Leck, C., Norman, M., Bigg, E. K., and Hillamo, R.: Chemical composition and sources of the high  
703 Arctic aerosol relevant for cloud formation, 107, *AAC 1-1-AAC 1-17*, 10.1029/2001jd001463,  
704 2002.

705 Levasseur, M.: Impact of Arctic meltdown on the microbial cycling of sulphur, *Nature Geoscience*, 6,  
706 691, 10.1038/ngeo1910, 2013.

707 Lindwall, F., Schollert, M., Michelsen, A., Blok, D., and Rinnan, R.: Fourfold higher tundra volatile  
708 emissions due to arctic summer warming, 121, 895-902, 10.1002/2015jg003295, 2016.

709 Mann, P. J., Spencer, R. G. M., Hernes, P. J., Six, J., Aiken, G. R., Tank, S. E., McClelland, J. W., Butler,  
710 K. D., Dyda, R. Y., and Holmes, R. M.: Pan-Arctic Trends in Terrestrial Dissolved Organic  
711 Matter from Optical Measurements, 4, 10.3389/feart.2016.00025, 2016.

712 Martin, M., Chang, R. Y. W., Sierau, B., Sjogren, S., Swietlicki, E., Abbatt, J. P. D., Leck, C., and  
713 Lohmann, U.: Cloud condensation nuclei closure study on summer arctic aerosol, *Atmos. Chem.*  
714 *Phys.*, 11, 11335-11350, 10.5194/acp-11-11335-2011, 2011.

715 Massicotte, P., Asmala, E., Stedmon, C., and Markager, S.: Global distribution of dissolved organic  
716 matter along the aquatic continuum: Across rivers, lakes and oceans, *Science of The Total*  
717 *Environment*, 609, 180-191, <https://doi.org/10.1016/j.scitotenv.2017.07.076>, 2017.

718 Mauritsen, T., Sedlar, J., Tjernström, M., Leck, C., Martin, M., Shupe, M., Sjogren, S., Sierau, B.,  
719 Persson, P. O. G., Brooks, I. M., and Swietlicki, E.: An Arctic CCN-limited cloud-aerosol regime,  
720 *Atmos. Chem. Phys.*, 11, 165-173, 10.5194/acp-11-165-2011, 2011.

721 Merikanto, J., Spracklen, D. V., Mann, G. W., Pickering, S. J., and Carslaw, K. S.: Impact of nucleation

on global CCN, *Atmos. Chem. Phys.*, 9, 8601-8616, 10.5194/acp-9-8601-2009, 2009.

Mungall, E. L., Croft, B., Lizotte, M., Thomas, J. L., Murphy, J. G., Levasseur, M., Martin, R. V., Wentzell, J. J. B., Liggio, J., and Abbatt, J. P. D.: Dimethyl sulfide in the summertime Arctic atmosphere: measurements and source sensitivity simulations, *Atmos. Chem. Phys.*, 16, 6665-6680, 10.5194/acp-16-6665-2016, 2016.

Németh, Z., and Salma, I.: Spatial extension of nucleating air masses in the Carpathian Basin, *Atmos. Chem. Phys.*, 14, 8841-8848, 10.5194/acp-14-8841-2014, 2014.

Nguyen, Q. T., Glasius, M., Sørensen, L. L., Jensen, B., Skov, H., Birmili, W., Wiedensohler, A., Kristensson, A., Nøjgaard, J. K., and Massling, A.: Seasonal variation of atmospheric particle number concentrations, new particle formation and atmospheric oxidation capacity at the high Arctic site Villum Research Station, Station Nord, *Atmos. Chem. Phys.*, 16, 11319-11336, 10.5194/acp-16-11319-2016, 2016.

O'Dowd, C., Ceburnis, D., Ovadnevaite, J., Vaishya, A., Rinaldi, M., and Facchini, M. C.: Do anthropogenic, continental or coastal aerosol sources impact on a marine aerosol signature at Mace Head?, *Atmos. Chem. Phys.*, 14, 10687-10704, 10.5194/acp-14-10687-2014, 2014.

O'Dowd, C. D., Jimenez, J. L., Bahreini, R., Flagan, R. C., Seinfeld, J. H., Hämeri, K., Pirjola, L., Kulmala, M., Jennings, S. G., and Hoffmann, T.: Marine aerosol formation from biogenic iodine emissions, *Nature*, 417, 632, 10.1038/nature00775, 2002.

Oziel, L., Neukermans, G., Ardyna, M., Lancelot, C., Tison, J.-L., Wassmann, P., Sirven, J., Ruiz-Pino, D., and Gascard, J.-C.: Role for Atlantic inflows and sea ice loss on shifting phytoplankton blooms in the Barents Sea, 122, 5121-5139, 10.1002/2016jc012582, 2017.

Pang, X., Pu, J., Zhao, X., Ji, Q., Qu, M., and Cheng, Z.: Comparison between AMSR2 Sea Ice Concentration Products and Pseudo-Ship Observations of the Arctic and Antarctic Sea Ice Edge on Cloud-Free Days, 10, 317, 2018.

Park, J., Dall'Osto, M., Park, K., Kim, J.-H., Park, J., Park, K.-T., Hwang, C. Y., Jang, G. I., Gim, Y., Kang, S., Park, S., Jin, Y. K., Yum, S. S., Simó, R., and Yoon, Y. J.: Arctic Primary Aerosol Production Strongly Influenced by Riverine Organic Matter, *Environmental Science & Technology*, 53, 8621-8630, 10.1021/acs.est.9b03399, 2019.

Park, K.-T., Lee, K., Kim, T.-W., Yoon, Y. J., Jang, E.-H., Jang, S., Lee, B.-Y., and Hermansen, O.: Atmospheric DMS in the Arctic Ocean and Its Relation to Phytoplankton Biomass, 32, 351-359, 10.1002/2017gb005805, 2018.

Park, K. T., Jang, S., Lee, K., Yoon, Y. J., Kim, M. S., Park, K., Cho, H. J., Kang, J. H., Udusti, R., Lee, B. Y., and Shin, K. H.: Observational evidence for the formation of DMS-derived aerosols during Arctic phytoplankton blooms, *Atmos. Chem. Phys.*, 17, 9665-9675, 10.5194/acp-17-9665-2017, 2017.

Peñuelas, J., and Staudt, M.: BVOCs and global change, *Trends in Plant Science*, 15, 133-144, <https://doi.org/10.1016/j.tplants.2009.12.005>, 2010.

Peters, G. P., Nilssen, T. B., Lindholt, L., Eide, M. S., Glomsrød, S., Eide, L. I., and Fuglestad, J. S.: Future emissions from shipping and petroleum activities in the Arctic, *Atmos. Chem. Phys.*, 11, 5305-5320, 10.5194/acp-11-5305-2011, 2011.

Peterson, B. J., Holmes, R. M., McClelland, J. W., Vörösmarty, C. J., Lammers, R. B., Shiklomanov, A. I., Shiklomanov, I. A., and Rahmstorf, S.: Increasing River Discharge to the Arctic Ocean, *Science*, 298, 2171-2173, 10.1126/science.1077445, 2002.

Pierce, J. R., Leitch, W. R., Liggio, J., Westervelt, D. M., Wainwright, C. D., Abbatt, J. P. D., Ahlm, L., Al-Basheer, W., Cziczo, D. J., Hayden, K. L., Lee, A. K. Y., Li, S. M., Russell, L. M., Sjostedt, S. J., Strawbridge, K. B., Travis, M., Vlasenko, A., Wentzell, J. J. B., Wiebe, H. A., Wong, J. P. S., and Macdonald, A. M.: Nucleation and condensational growth to CCN sizes during a sustained pristine biogenic SOA event in a forested mountain valley, *Atmos. Chem. Phys.*, 12, 3147-3163, 10.5194/acp-12-3147-2012, 2012.

Pierce, J. R., Westervelt, D. M., Atwood, S. A., Barnes, E. A., and Leitch, W. R.: New-particle formation, growth and climate-relevant particle production in Egbert, Canada: analysis from 1

773 [year of size-distribution observations](#), *Atmos. Chem. Phys.*, 14, 8647-8663, 10.5194/acp-14-  
774 8647-2014, 2014.

775 Potosnak, M. J., Baker, B. M., LeSturgeon, L., Disher, S. M., Griffin, K. L., Bret-Harte, M. S., and  
776 Starr, G.: Isoprene emissions from a tundra ecosystem, *Biogeosciences*, 10, 871-889,  
777 10.5194/bg-10-871-2013, 2013.

778 Quinn, P. K., and Bates, T. S.: The case against climate regulation via oceanic phytoplankton sulphur  
779 emissions, *Nature*, 480, 51-56, 10.1038/nature10580, 2011.

780 Quinn, P. K., Collins, D. B., Grassian, V. H., Prather, K. A., and Bates, T. S.: Chemistry and Related  
781 Properties of Freshly Emitted Sea Spray Aerosol, *Chemical Reviews*, 115, 4383-4399,  
782 10.1021/cr500713g, 2015.

783 Raso, A. R. W., Custard, K. D., May, N. W., Tanner, D., Newburn, M. K., Walker, L., Moore, R. J., Huey,  
784 L. G., Alexander, L., Shepson, P. B., and Pratt, K. A.: Active molecular iodine photochemistry in  
785 the Arctic, *Proceedings of the National Academy of Sciences*, 114, 10053-10058,  
786 10.1073/pnas.1702803114, 2017.

787 Rose, C., Sellegri, K., Moreno, I., Velarde, F., Ramonet, M., Weinhold, K., Krejci, R., Andrade, M.,  
788 Wiedensohler, A., Ginot, P., and Laj, P.: CCN production by new particle formation in the free  
789 troposphere, *Atmos. Chem. Phys.*, 17, 1529-1541, 10.5194/acp-17-1529-2017, 2017.

790 Schmale, J., Arnold, S. R., Law, K. S., Thorp, T., Anenberg, S., Simpson, W. R., Mao, J., and Pratt, K.  
791 A.: Local Arctic Air Pollution: A Neglected but Serious Problem, 6, 1385-1412,  
792 10.1029/2018ef000952, 2018a.

793 Schmale, J., Henning, S., Decesari, S., Henzing, B., Keskinen, H., Sellegri, K., Ovadnevaite, J., Pöhlker,  
794 M. L., Brito, J., Bougiatioti, A., Kristensson, A., Kalivitis, N., Stavroulas, I., Carbone, S.,  
795 Jefferson, A., Park, M., Schlag, P., Iwamoto, Y., Aalto, P., Äijälä, M., Bukowiecki, N., Ehn, M.,  
796 Frank, G., Fröhlich, R., Frumau, A., Herrmann, E., Herrmann, H., Holzinger, R., Kos, G.,  
797 Kulmala, M., Mihalopoulos, N., Nenes, A., O'Dowd, C., Petäjä, T., Picard, D., Pöhlker, C.,  
798 Pöschl, U., Poulain, L., Prévôt, A. S. H., Swietlicki, E., Andreae, M. O., Artaxo, P., Wiedensohler,  
799 A., Ogren, J., Matsuki, A., Yum, S. S., Stratmann, F., Baltensperger, U., and Gysel, M.: Long-  
800 term cloud condensation nuclei number concentration, particle number size distribution and  
801 chemical composition measurements at regionally representative observatories, *Atmos. Chem.*  
802 *Phys.*, 18, 2853-2881, 10.5194/acp-18-2853-2018, 2018b.

803 Schollert, M., Burchard, S., Faubert, P., Michelsen, A., and Rinnan, R. J. P. B.: Biogenic volatile organic  
804 compound emissions in four vegetation types in high arctic Greenland, 37, 237-249,  
805 10.1007/s00300-013-1427-0, 2014.

806 Sellegri, K., O'Dowd, C. D., Yoon, Y. J., Jennings, S. G., and Leeuw, G. d.: Surfactants and submicron  
807 sea spray generation, *Journal of Geophysical Research: Atmospheres*, 111,  
808 doi:10.1029/2005JD006658, 2006.

809 Shen, Y., Fichot, C., and Benner, R.: Dissolved organic matter composition and bioavailability reflect  
810 ecosystem productivity in the Western Arctic Ocean, 2012.

811 Shiklomanov, I. A., Shiklomanov, A. I., Lammers, R. B., Peterson, B. J., and Vorosmarty, C. J.: The  
812 Dynamics of River Water Inflow to the Arctic Ocean, in: *The Freshwater Budget of the Arctic*  
813 *Ocean*, edited by: Lewis, E. L., Jones, E. P., Lemke, P., Prowse, T. D., and Wadhams, P.,  
814 Springer Netherlands, Dordrecht, 281-296, 2000.

815 Spracklen, D. V., Carslaw, K. S., Kulmala, M., Kerminen, V.-M., Sihto, S.-L., Riipinen, I., Merikanto, J.,  
816 Mann, G. W., Chipperfield, M. P., Wiedensohler, A., Birmili, W., and Lihavainen, H.:  
817 Contribution of particle formation to global cloud condensation nuclei concentrations,  
818 *Geophysical Research Letters*, 35, doi:10.1029/2007GL033038, 2008.

819 Steinke, M., Hodapp, B., Subhan, R., Bell, T. G., and Martin-Creuzburg, D.: Flux of the biogenic  
820 volatiles isoprene and dimethyl sulfide from an oligotrophic lake, *Scientific Reports*, 8, 630,  
821 10.1038/s41598-017-18923-5, 2018.

822 Stier, P., Seinfeld, J. H., Kinne, S., and Boucher, O.: Aerosol absorption and radiative forcing, *Atmos.*  
823 *Chem. Phys.*, 7, 5237-5261, 10.5194/acp-7-5237-2007, 2007.

- 824 Stroeve, J. C., Serreze, M. C., Holland, M. M., Kay, J. E., Malanik, J., and Barrett, A. P.: The Arctic's  
825 rapidly shrinking sea ice cover: a research synthesis, *Climatic Change*, 110, 1005-1027,  
826 10.1007/s10584-011-0101-1, 2012.
- 827 Ström, J., Umegård, J., Tørseth, K., Tunved, P., Hansson, H. C., Holmén, K., Wismann, V., Herber, A.,  
828 and König-Langlo, G.: One year of particle size distribution and aerosol chemical composition  
829 measurements at the Zeppelin Station, Svalbard, March 2000–March 2001, *Physics and  
830 Chemistry of the Earth, Parts A/B/C*, 28, 1181-1190, <https://doi.org/10.1016/j.pce.2003.08.058>,  
831 2003.
- 832 Suni, T., Kulmala, M., Hirsikko, A., Bergman, T., Laakso, L., Aalto, P. P., Leuning, R., Cleugh, H.,  
833 Zegelin, S., Hughes, D., van Gorsel, E., Kitchen, M., Vana, M., Hörrak, U., Mirme, S., Mirme,  
834 A., Sevanto, S., Twining, J., and Tadros, C.: Formation and characteristics of ions and charged  
835 aerosol particles in a native Australian Eucalypt forest, *Atmos. Chem. Phys.*, 8, 129-139,  
836 10.5194/acp-8-129-2008, 2008.
- 837 Svenningsson, B., Arneth, A., Hayward, S., Holst, T., Massling, A., Swietlicki, E., Hirsikko, A.,  
838 Junninen, H., Riipinen, I., Vana, M., Maso, M. D., Hussein, T., and Kulmala, M.: Aerosol  
839 particle formation events and analysis of high growth rates observed above a subarctic wetland–  
840 forest mosaic, *Tellus B: Chemical and Physical Meteorology*, 60, 353-364, 10.1111/j.1600-  
841 0889.2008.00351.x, 2008.
- 842 TAPE, K., STURM, M., and RACINE, C.: The evidence for shrub expansion in Northern Alaska and  
843 the Pan-Arctic, 12, 686-702, 10.1111/j.1365-2486.2006.01128.x, 2006.
- 844 Tremblay, S., Picard, J.-C., Bachelder, J. O., Lutsch, E., Strong, K., Fogal, P., Leitch, W. R., Sharma, S.,  
845 Kolonjari, F., Cox, C. J., Chang, R. Y.-W., and Hayes, P. L.: Characterization of aerosol growth  
846 events over Ellesmere Island during the summers of 2015 and 2016, *Atmos. Chem. Phys.*, 19,  
847 5589–5604, <https://doi.org/10.5194/acp-19-5589-2019>, 2019.
- 848 Tunved, P., Ström, J., and Krejci, R.: Arctic aerosol life cycle: linking aerosol size distributions  
849 observed between 2000 and 2010 with air mass transport and precipitation at Zeppelin station,  
850 Ny-Ålesund, Svalbard, *Atmos. Chem. Phys.*, 13, 3643-3660, 10.5194/acp-13-3643-2013, 2013.
- 851 Twomey, S.: Pollution and the planetary albedo, *Atmospheric Environment (1967)*, 8, 1251-1256,  
852 [https://doi.org/10.1016/0004-6981\(74\)90004-3](https://doi.org/10.1016/0004-6981(74)90004-3), 1974.
- 853 Väänänen, R., Kyrö, E. M., Nieminen, T., Kivekäs, N., Junninen, H., Virkkula, A., Dal Maso, M.,  
854 Lihavainen, H., Viisanen, Y., Svenningsson, B., Holst, T., Arneth, A., Aalto, P. P., Kulmala, M.,  
855 and Kerminen, V. M.: Analysis of particle size distribution changes between three measurement  
856 sites in northern Scandinavia, *Atmos. Chem. Phys.*, 13, 11887-11903, 10.5194/acp-13-11887-  
857 2013, 2013.
- 858 Vana, M., Kulmala, M., Dal Maso, M., Hörrak, U., and Tamm, E.: Comparative study of nucleation  
859 mode aerosol particles and intermediate air ions formation events at three sites, 109,  
860 10.1029/2003jd004413, 2004.
- 861 Vehkamäki, H., Dal Maso, M., Hussein, T., Flanagan, R., Hyvärinen, A., Lauros, J., Merikanto, P.,  
862 Mönkkönen, M., Pihlatie, K., Salminen, K., Sogacheva, L., Thum, T., Ruuskanen, T. M.,  
863 Keronen, P., Aalto, P. P., Hari, P., Lehtinen, K. E. J., Rannik, Ü., and Kulmala, M.: Atmospheric  
864 particle formation events at Värriö measurement station in Finnish Lapland 1998-2002, *Atmos.  
865 Chem. Phys.*, 4, 2015-2023, 10.5194/acp-4-2015-2004, 2004.
- 866 Wang, M., and Overland, J. E.: A sea ice free summer Arctic within 30 years?, *Geophysical Research  
867 Letters*, 36, doi:10.1029/2009GL037820, 2009.
- 868 Watson, J. G., Chow, J. C., Sodeman, D. A., Lowenthal, D. H., Chang, M. C. O., Park, K., and Wang,  
869 X.: Comparison of four scanning mobility particle sizers at the Fresno Supersite, *Particuology*, 9,  
870 204-209, 2011.
- 871 Westervelt, D. M., Pierce, J. R., and Adams, P. J.: Analysis of feedbacks between nucleation rate,  
872 survival probability and cloud condensation nuclei formation, *Atmos. Chem. Phys.*, 14, 5577-  
873 5597, 10.5194/acp-14-5577-2014, 2014.
- 874 Willis, M. D., Burkart, J., Thomas, J. L., Köllner, F., Schneider, J., Bozem, H., Hoor, P. M., Aliabadi, A.

875 A., Schulz, H., Herber, A. B., Leaitch, W. R., and Abbatt, J. P. D.: Growth of nucleation mode  
876 particles in the summertime Arctic: a case study, *Atmos. Chem. Phys.*, 7663-7679, 10.5194/acp-  
877 16-7663-2016, 2016.

878 Willis, M. D., Leaitch, W. R., and Abbatt, J. P. D.: Processes Controlling the Composition and  
879 Abundance of Arctic Aerosol, *56*, 621-671, 10.1029/2018rg000602, 2018.

880 Yum, S. S., Hudson, J. G., and Xie, Y.: Comparisons of cloud microphysics with cloud condensation  
881 nuclei spectra over the summertime Southern Ocean, *103*, 16625-16636, 10.1029/98jd01513,  
882 1998.

883 Zhang, R., Khalizov, A., Wang, L., Hu, M., and Xu, W.: Nucleation and Growth of Nanoparticles in the  
884 Atmosphere, *Chemical Reviews*, 112, 1957-2011, 10.1021/cr2001756, 2012.

885 Ziemba, L. D., Dibb, J. E., Griffin, R. J., Huey, L. G., and Beckman, P.: Observations of particle growth  
886 at a remote, Arctic site, *Atmos. Environ.*, 44, 1649–1657,  
887 <https://doi.org/10.1016/j.atmosenv.2010.01.032>, 2010.

888

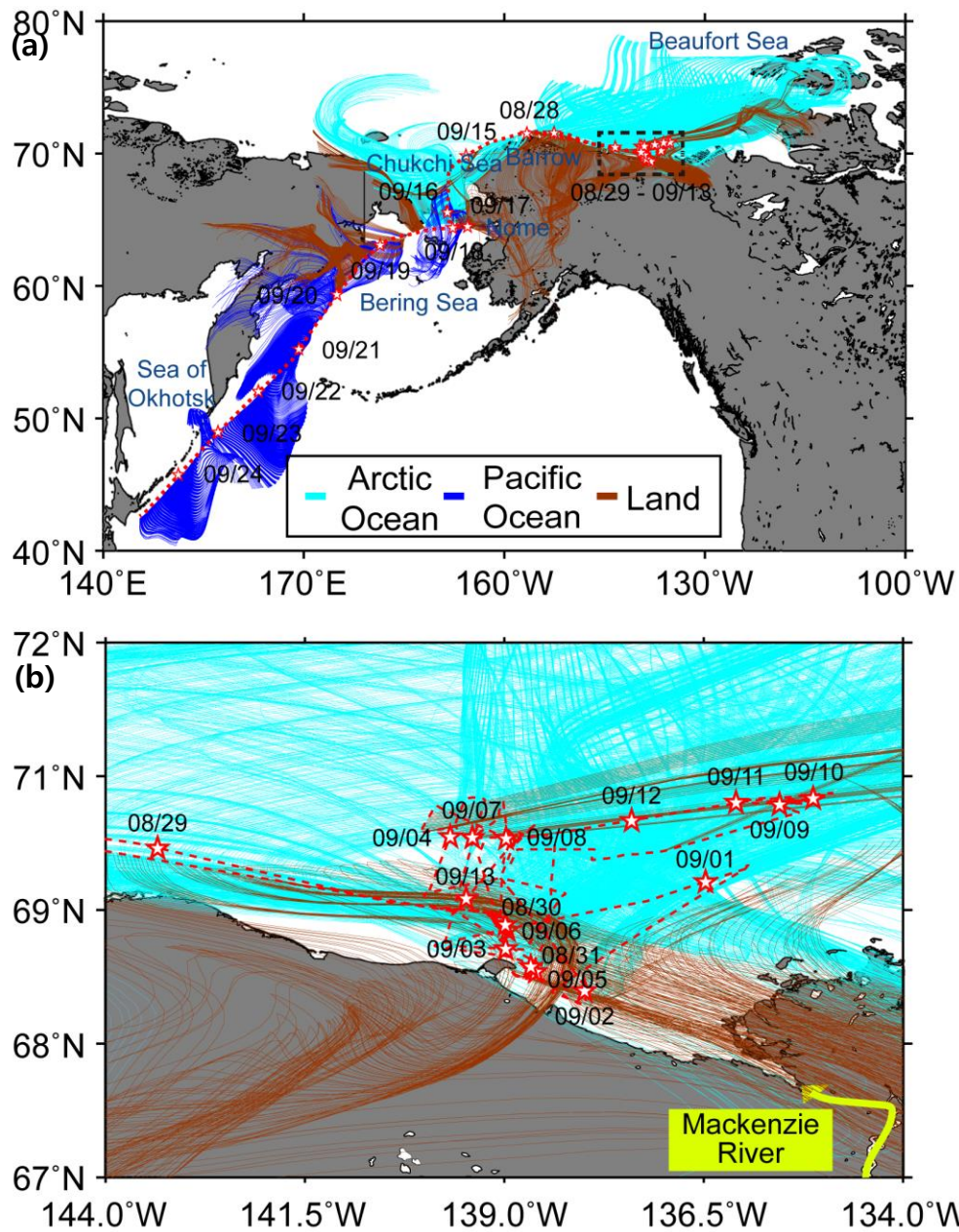
889

890 Table 1. A summary of meteorology, total number concentrations of particles (measured with TSI 3776  
 891 CPC, TSI 3772 CPC, Standard SMPS, nano SMPS), growth rate (GR), and condensation sink (CS) for  
 892 the three selected periods. The CN<sub>2.5</sub> and CN<sub>10</sub> represents the total number concentration of particles  
 893 larger than 2.5 nm and 10 nm, respectively. The N<sub>NUC</sub>, N<sub>AIT</sub>, N<sub>ACC</sub>, and N<sub>OPS</sub> represents total aerosol  
 894 nucleation-mode (3 – 20 nm), Aitken-mode (20 – 100 nm), accumulation-mode (100 – 300 nm), and  
 895 coarse-mode (> 300 nm from OPS) number concentrations.

	Arctic Marine	Arctic Terrestrial	Pacific Ocean
Periods	9/02/2017– 9/05/2017, 9/10/2017– 9/12/2017	9/13/2017– 9/17/2017	9/21/2017– 9/23/2017
Wind speed (m s <sup>-1</sup> )	6.1 ± 6.0	8.7 ± 5.7	8.4 ± 4.3
Wind direction (°)	352.3 ± 38.7	344.7 ± 28.1	338.3 ± 23.0
CN <sub>2.5</sub> (cm <sup>-3</sup> )	413 ± 442	1622 ± 1450	397 ± 185
CN <sub>10</sub> (cm <sup>-3</sup> )	414 ± 452	1396 ± 1279	384 ± 86
CN <sub>2.5-10</sub> (cm <sup>-3</sup> )	62 ± 130	263 ± 318	35 ± 195
N <sub>NUC</sub> (cm <sup>-3</sup> )	118 ± 198	350 ± 393	46 ± 103
N <sub>AIT</sub> (cm <sup>-3</sup> )	108 ± 132	405 ± 425	116 ± 93
N <sub>ACC</sub> (cm <sup>-3</sup> )	19 ± 14	33 ± 20	95 ± 30
N <sub>OPS</sub> (cm <sup>-3</sup> )	2 ± 2	3 ± 2	11 ± 6
GR (nm h <sup>-1</sup> )	0.4 ± 0.3	0.8 ± 0.2	-
CS (h <sup>-1</sup> )	0.5 ± 0.4	0.9 ± 0.5	2.1 ± 0.7

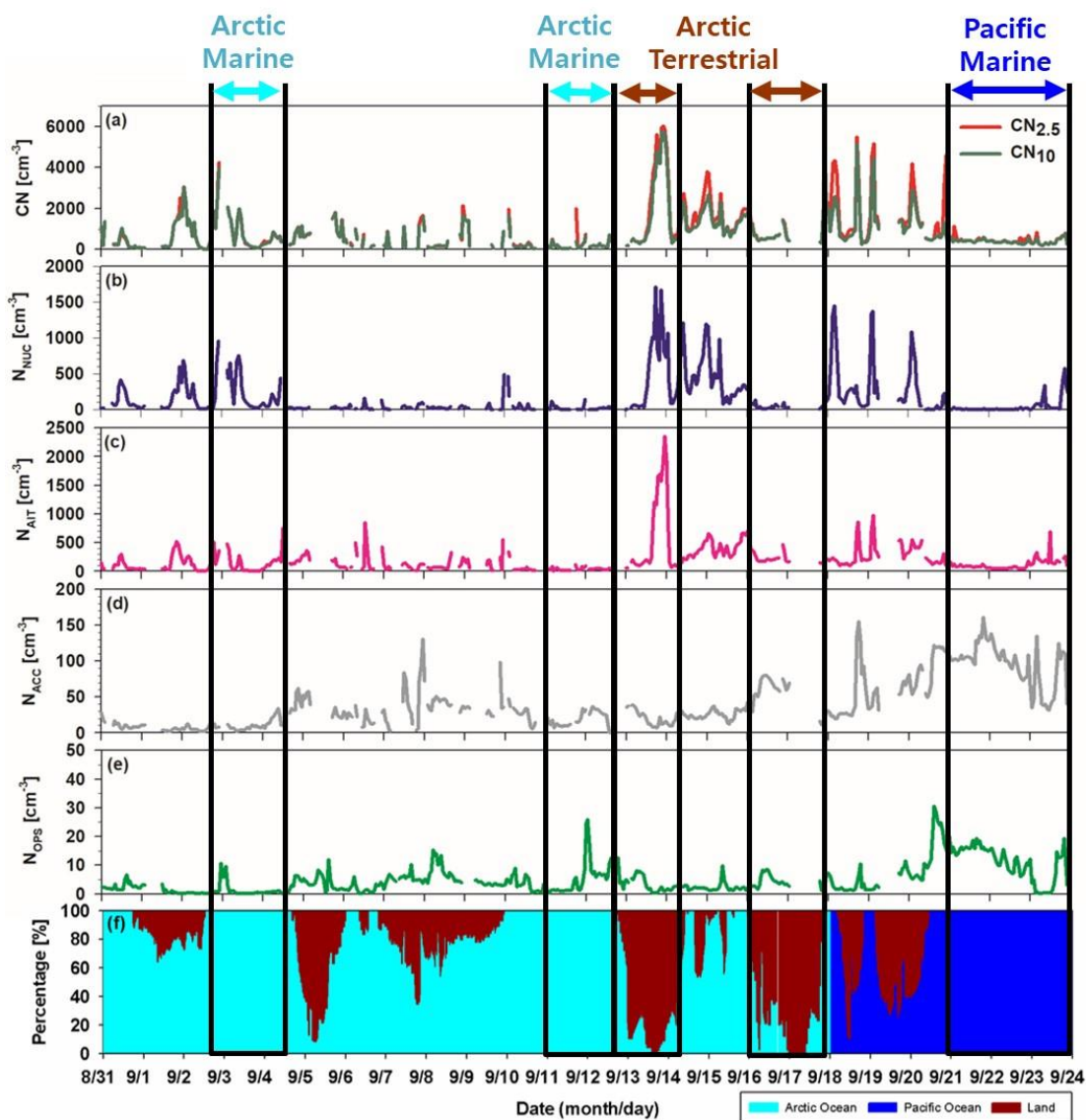
896

897



898

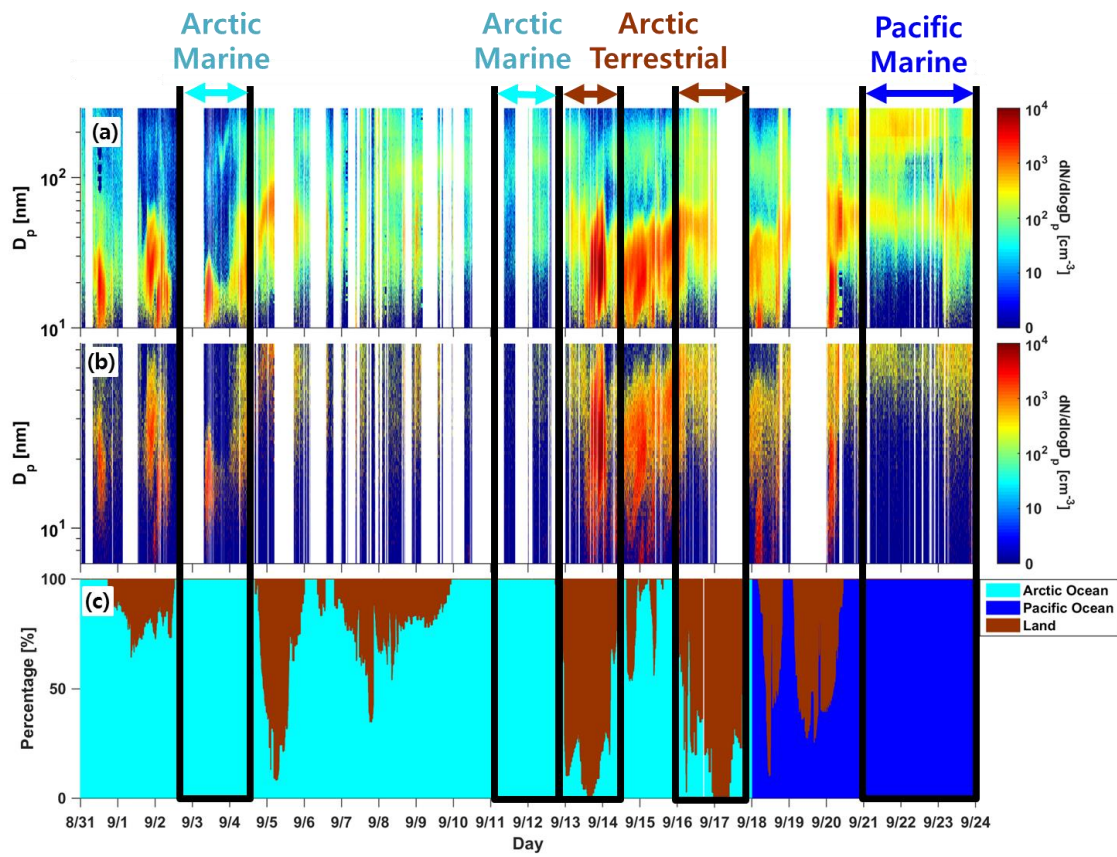
899 Figure 1. Ship tracks across (a) the Arctic (8/28/2017–9/18/2017) and Pacific Oceans  
 900 (9/18/2017–9/25/2017) and (b) zoom into the dotted black square region in Fig. 1a. A dotted red line  
 901 including star symbols represents ship tracks during the entire cruise. The star symbols represent the  
 902 daily ship location at midnight. Light blue, blue and brown lines denote the 2-day air mass trajectories  
 903 categorized into three main domains such as Arctic Ocean, Pacific Ocean, and land, respectively.



905

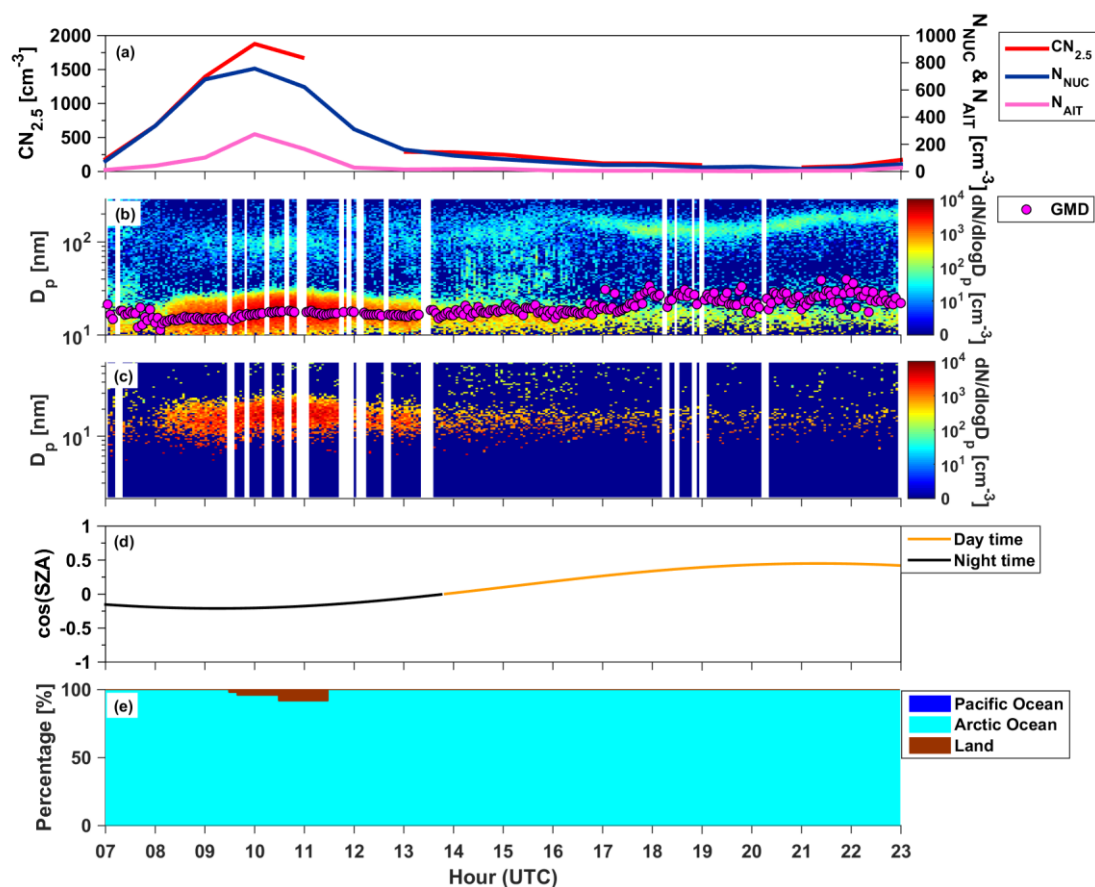
906 Figure 2. Time series of the 1 hour average (a) total aerosol ( $CN_{2.5}$  and  $CN_{10}$ ), (b) nucleation-mode (3 –  
 907 20 nm) ( $N_{NUC}$ ), (c) Aitken-mode (20 – 100 nm) ( $N_{AIT}$ ), (d) accumulation-mode (100 – 300 nm) ( $N_{ACC}$ ),  
 908 (e) coarse-mode (> 300 nm from OPS) ( $N_{OPS}$ ) number concentrations, and (f) the residence time of air  
 909 masses that passed over the Arctic Ocean, Pacific Ocean, and land. The  $CN_{2.5}$  and  $CN_{10}$  represent total  
 910 number concentration of particles larger than 2.5 and 10 nm, respectively.

911



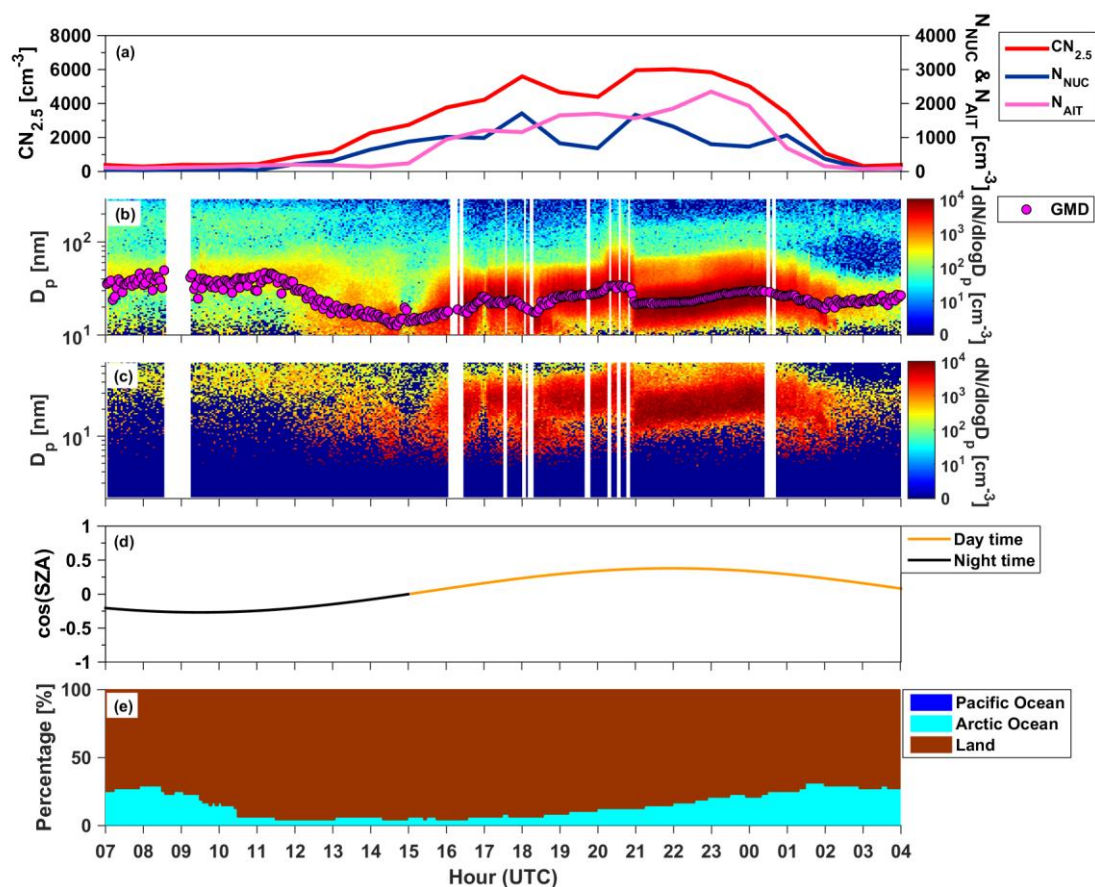
913

914 Figure 3. Contour plots of the size distributions measured using (a) standard and (b) nano SMPS and (c)  
 915 the residence time of air masses that passed over the Arctic Ocean, Pacific Ocean, and land throughout  
 916 the sampling periods.



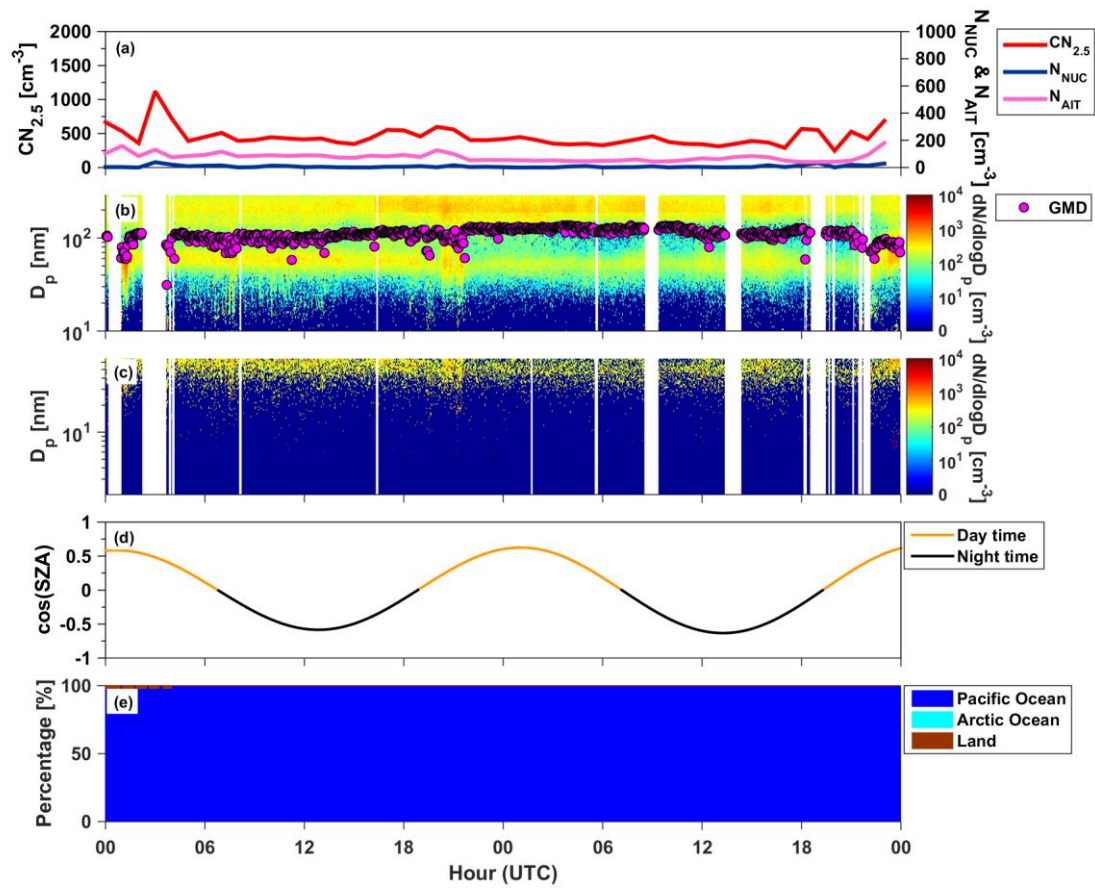
918

919 Figure 4. Example of a case-I event observed on 3 September 2017. From top to bottom, the parameters  
 920 are: (a) the total number concentration of particles smaller than 2.5 nm, nucleation-mode particles, and  
 921 Aitken-mode particles; (b) a time series of the standard SMPS size distribution and GMD; (c) a time  
 922 series of the nano SMPS size; (d) Cosine values of solar zenith angle; (e) the residence time of air  
 923 masses that passed over the ocean, land, and sea-ice areas.



925

926 Figure 5. Example of a case II event that was observed on September 13–14, 2017. From top to bottom,  
 927 the parameters are: (a) the total number concentration of particles smaller than 2.5 nm, nucleation-mode  
 928 particles, and Aitken-mode particles; (b) a time series of the standard SMPS size distribution and GMD;  
 929 (c) a time series of the nano SMPS size; (d) cosine values of solar zenith angle; (e) the residence time of  
 930 air masses that passed over the ocean, land, and sea-ice areas.



932

933 Figure 6. Example of a case III event that was observed on September 21–22 2017. From top to bottom,

934 the parameters are: (a) the total number concentration of particles smaller than 2.5 nm, nucleation-mode

935 particles, and Aitken-mode particles; (b) a time series of the standard SMPS size distribution and GMD;

936 (c) a time series of the nano SMPS size; (d) cosine values of solar zenith angle; (e) the residence time of

937 air masses that passed over the ocean, land, and sea-ice areas.

938

939  
940  
941  
942  
943  
944  
945  
946  
947  
948  
949  
950

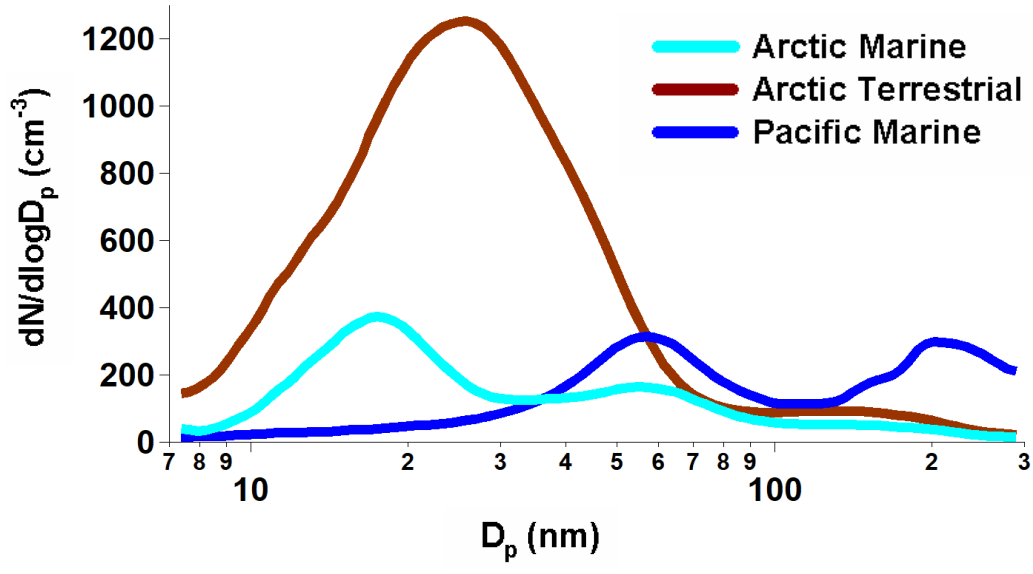
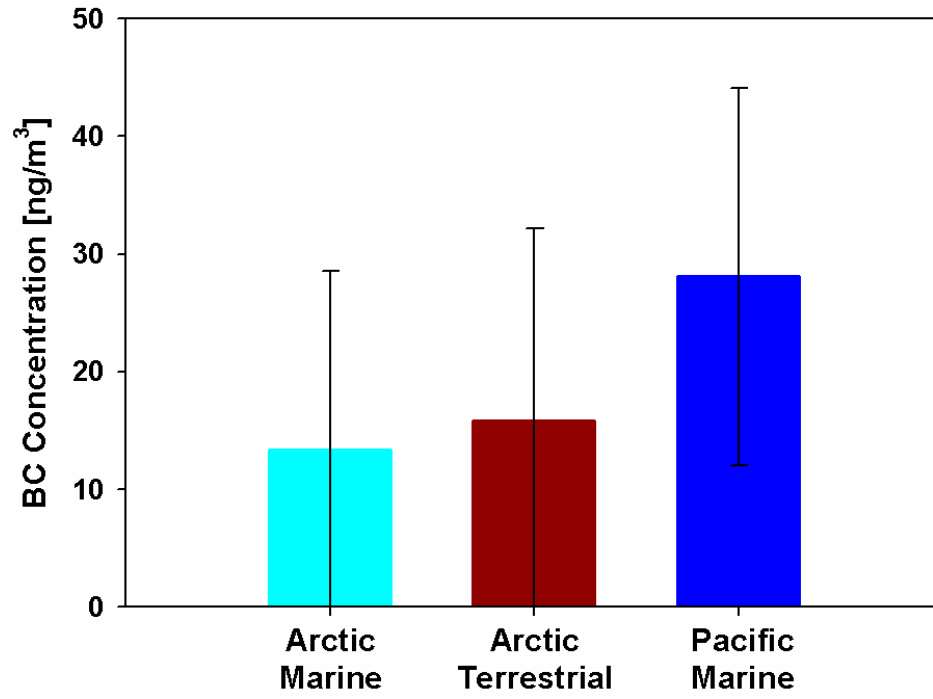
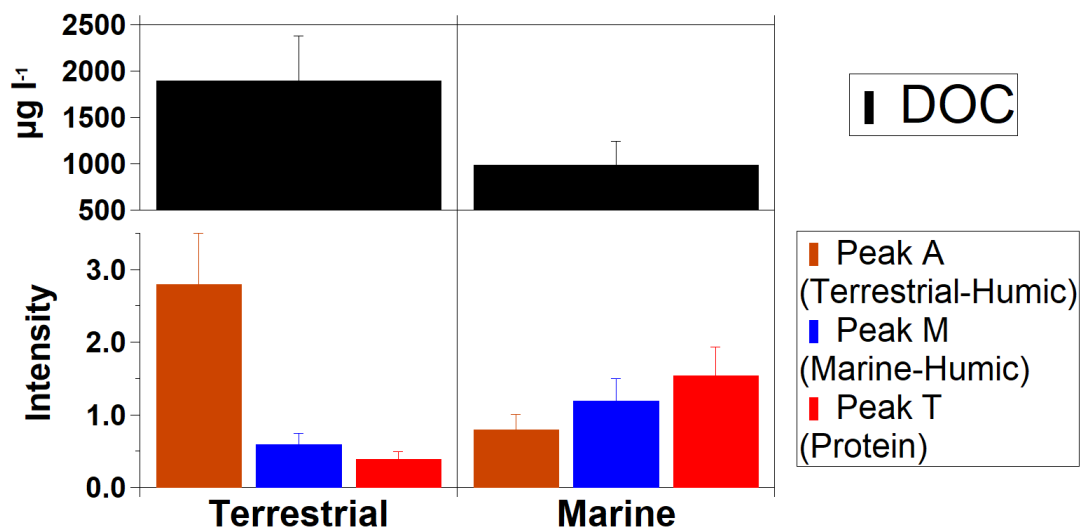


Figure 7. Average size distributions of aerosol particles for Arctic marine, Arctic terrestrial and Pacific marine air masses



952

953 Figure 8. Average mass concentrations of black carbon for each air mass.



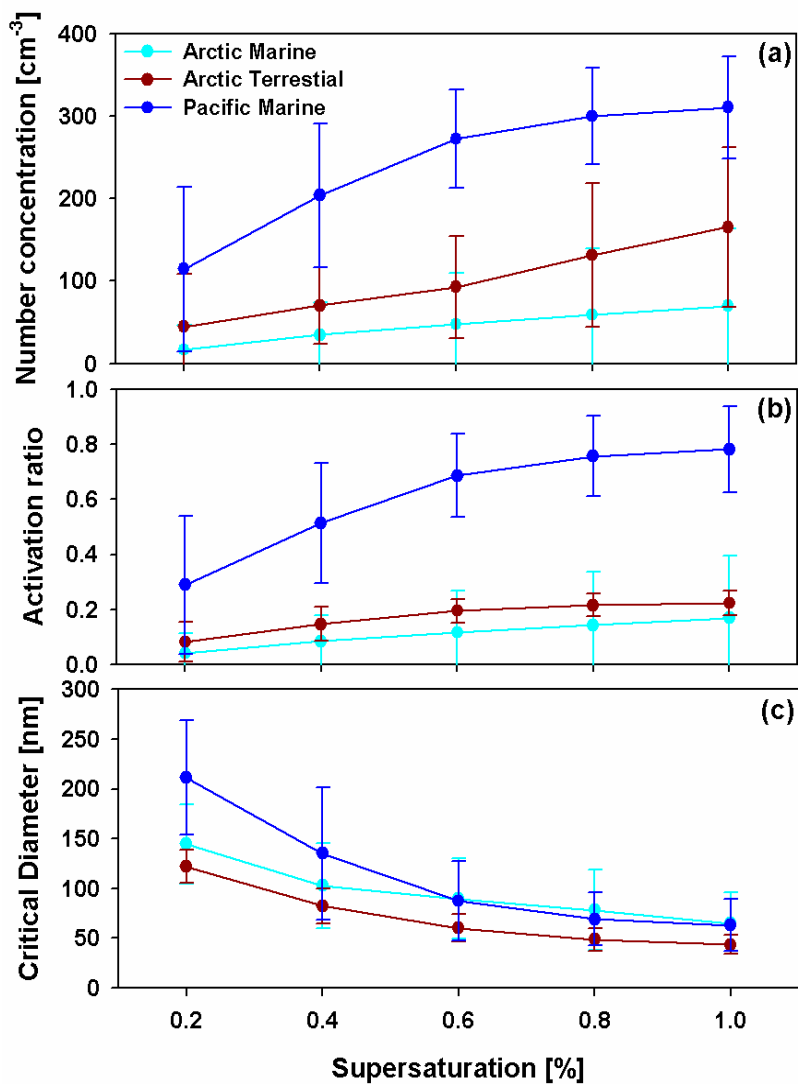
955

956 Figure 9. Average DOC concentrations for surface seawater samples collected during this cruise,  
 957 simultaneously during the atmospheric measurements herein reported. Peak A, M, and T represent  
 958 terrestrial-humic substances, marine-fulvic substances, and protein, respectively.

959

960

961



963

964 Figure 10. Comparisons of (a) CCN number concentrations, (b) CCN activity, and (c) critical diameter  
 965 for Arctic marine, Arctic terrestrial and Pacific marine air masses under different supersaturation  
 966 conditions. The error bars represent a standard deviation.